

Published in final edited form as:

Development ; 146(22): . doi:10.1242/dev.174565.

Centrosome Aurora A regulates RhoGEF ECT-2 localisation and ensures a single PAR-2 polarity axis in *C. elegans* embryos

Sukriti Kapoor, Sachin Kotak*

Department of Microbiology and Cell Biology (MCB), Indian Institute of Science, Bangalore 560012, India

Abstract

Proper establishment of cell polarity is essential for development. In the one-cell *C. elegans* embryo, a centrosome-localised signal provides spatial information for polarity establishment. It is hypothesised that this signal causes local inhibition of the cortical actomyosin network, and breaks symmetry to direct partitioning of the PAR proteins. However, the molecular nature of the centrosomal signal that triggers cortical anisotropy in the actomyosin network to promote polarity establishment remains elusive. Here, we discover that depletion of Aurora A kinase (AIR-1 in *C. elegans*) causes pronounced cortical contractions on the embryo surface, and this creates more than one PAR-2 polarity axis. This function of AIR-1 appears to be independent of its role in microtubule nucleation. Importantly, upon AIR-1 depletion, centrosome positioning becomes dispensable in dictating the PAR-2 axis. Moreover, we uncovered that a Rho GEF, ECT-2, acts downstream of AIR-1 in regulating contractility and PAR-2 localisation, and, notably, AIR-1 depletion influences ECT-2 cortical localisation. Overall, this study provides a novel insight into how an evolutionarily conserved centrosome Aurora A kinase inhibits promiscuous PAR-2 domain formation to ensure singularity in the polarity establishment axis.

Keywords

Aurora A; PAR proteins; Rho GEF; Actomyosin; Centrosomes; Polarity establishment

Introduction

Proper establishment of cell polarity is vital for several events during development and morphogenesis. Myriad distinct signals are deployed by various cell types to trigger polarity formation (reviewed by Chant, 1999; Nelson, 2003). The one-cell stage of the *Caenorhabditis elegans* embryo has proven to be an excellent system for investigating the mechanisms of polarity establishment. In this remarkable cell, centrosomes play a crucial

* Author for correspondence (sachinkotak@iisc.ac.in).

Competing interests

The authors declare no competing or financial interests.

Author contributions

Conceptualization: S. Kotak; Methodology: S. Kapoor, S. Kotak; Validation: S. Kapoor, S. Kotak; Formal analysis: S. Kapoor, S. Kotak; Investigation: S. Kapoor, S. Kotak; Resources: S. Kotak; Data curation: S. Kapoor, S. Kotak; Writing - original draft: S. Kotak; Writing - review & editing: S. Kapoor, S. Kotak; Visualization: S. Kapoor, S. Kotak; Supervision: S. Kotak; Project administration: S. Kotak; Funding acquisition: S. Kotak.

function in symmetry breaking and thus setting up polarity (Cowan and Hyman, 2004; reviewed by Hoegge and Hyman, 2013; Motegi and Seydoux, 2013; Rose and Gönczy, 2014). It has been suggested that the pericentriolar material (PCM) proteins of the centrosome are needed for polarity establishment (Goldstein and Hird, 1996; O'Connell et al., 2000; Hamill et al., 2002). Furthermore, the microtubules are also linked in regulating proper polarity in the one-cell embryo (Wallenfang and Seydoux, 2000; Tsai and Ahringer, 2007; reviewed by Siegrist and Doe, 2007).

Functional characterisation of several mutants indicates that centrosome-cortical distance is correlated with the defects in polarity establishment (Rappleye et al., 2002, 2003; Fortin et al., 2010). Interestingly, it has been shown that centrosomes are capable of initiating polarity from any position in the one-cell embryo, though the proximity of the centrosome to the cell cortex is a crucial determinant for the timing of polarity initiation (Bienkowska and Cowan, 2012). This study also proposes that the centrosome carries a gradient of a diffusive signal that acts as a molecular ruler to instruct polarity establishment at the closest cell cortex. However, the nature of such a polarity-initiation signal remains elusive.

How does the centrosome instruct the neighbouring cell cortex to establish cell polarity? It has been proposed that the local inhibition of the actomyosin contractions in the vicinity of centrosome provides the trigger to commence anisotropy (Munro et al., 2004; reviewed in Cowan and Hyman, 2007). This event leads to the formation of localised domains of the partition defective proteins [the aPARs: PAR-3, PAR-6 and atypical protein kinase C (aPKC), and the pPARs: PAR-1, PAR-2 and LGL] (reviewed by Motegi and Seydoux, 2013; Hoegge and Hyman, 2013). Mutants defective for actomyosin-based contractility are impaired in establishing polarity (Guo and Kemphues, 1996; Hill and Strome, 1990; Severson and Bowerman, 2003). However, the initiation of contractile asymmetry is independent of PAR polarity; for example, PAR-6 can localise asymmetrically at the anterior cortex in *par-2 (RNAi)* embryos (Cuenca et al., 2003; Goehring et al., 2011). A small GTPase, RHO-1, and its activator RhoGEF ECT-2 play a crucial role in controlling contractile asymmetry by modulating the actomyosin network (Motegi and Sugimoto, 2006). RNAi-mediated depletion of ECT-2 or its activator NOP-1 abolishes cortical contractility (Motegi and Sugimoto, 2006; Tse et al., 2012). In such embryos, the pPAR domain eventually forms, possibly because of a redundant microtubule-dependent polarity pathway that operates at the time of polarity maintenance (Zonies et al., 2010; Motegi et al., 2011; Tse et al., 2012; reviewed by Motegi and Seydoux, 2013; Rose and Gönczy, 2014). Notably, ECT-2 is excluded from the posterior cortex at the onset of symmetry breaking, and this event is correlated with the disappearance of the non-muscle myosin II (NMY-2) from the posterior cortex (Munro et al., 2004; Motegi and Sugimoto, 2006). However, the molecular pathway that delocalises ECT-2 and consequently establishes polarity remains unknown.

Depletion of the PP6 phosphatase catalytic subunit PPH-6 or its regulatory subunit SAPS-1 decreases cortical contractility and causes the disappearance of pseudocleavage in the one-cell embryo (Afshar et al., 2010). We have previously shown that SAPS-1 interacts with Aurora A kinase (AIR-1), and the interplay between AIR-1 and SAPS-1 is crucial for mitotic spindle positioning in the one-cell embryo (Kotak et al., 2016). AIR-1 is a serine/threonine kinase that is essential for the timely mitotic entry, centrosome separation,

centrosome maturation, spindle assembly, spindle positioning, spindle elongation and cytokinesis (Hannak et al., 2001; Giet et al., 2002; Toji et al., 2004; Tsai and Zheng, 2005; Hachet et al., 2007; Portier et al., 2007; Seki et al., 2008; Wong et al., 2008; Zhang et al., 2008; Reboutier et al., 2013; Kotak et al., 2016; Mangal et al., 2018). Auto-phosphorylation of AIR-1 at threonine 201 (threonine 288 in humans) in its activation loop increases the catalytic activity of Aurora A (Walter et al., 2000; Littlepage et al., 2002; Toya et al., 2011). Interestingly, biochemical and cell biological data suggest that, in human cells, PP6 phosphatase acts as a T-loop phosphatase for T288 of Aurora A and keeps its activity in a balanced state for proper spindle assembly (Zeng et al., 2010).

In the present work, we show that, in contrast to PP6 phosphatase, loss of AIR-1 causes excess cortical contractility at the time of polarity initiation. This translates into polarity defects where more than one pPAR axis is set up in the one-cell embryo. We show that this function of AIR-1 is dependent on its autocatalytic activity, but not its co-activator TPXL-1 (TPX-2 in humans). Notably, we uncovered that AIR-1 controls pPAR polarity independently of its role in regulating microtubule nucleation at the centrosome. Interestingly, loss of AIR-1 makes the centrosome dispensable in choreographing the position of polarity establishment. We further reveal that AIR-1 is required to exclude ECT-2 from the posterior cortex in a timely manner. Overall, our study provides a mechanism by which centrosomal AIR-1 promotes singularity in polarisation by locally excluding ECT-2 at the posterior cortex.

Results

Loss of AIR-1 causes excess cortical contractility in the one-cell embryo

PPH-6 phosphatase and its regulatory subunit SAPS-1 influences cortical contractility in the one-cell stage of *C. elegans* embryo during symmetry-breaking phase (henceforth referred to as polarity establishment) by modulating the cortical organisation of nonmuscle myosin II (NMY-2) (compare Fig. 1B with 1A; Movies 1 and 2) (Afshar et al., 2010). SAPS-1 interacts with AIR-1 (Kotak et al., 2016); therefore, we characterised the influence of AIR-1 depletion on cortical contractility in early one-cell embryos at the time of polarity setup. RNAi-mediated AIR-1 depletion impacts centrosome maturation and leads to a significant decrease in the centrosomal tubulin fluorescence, which results in collapsing of the centrosomes after nuclear envelope breakdown (NEBD) during prophase (Hannak et al., 2001; Fig. S1A,B,E; Movies 3 and 4). Thus, we chose this RNAi condition for further experiments. Notably, RNAi-based loss of AIR-1 causes exaggerated cortical contractility at the time of polarity establishment, which is antagonistic to SAPS-1 depletion (compare Fig. 1C with 1A and 1B; Movie 5).

In mammalian cells, the PPH-6 homologue PP6 de-phosphorylates Aurora A at T288 (T201 in AIR-1; Toya et al., 2011) to modulate Aurora A activity for proper spindle assembly (Zeng et al., 2010). Therefore, we postulated that SAPS-1 could be modulating AIR-1 activity for proper cortical contractility. If this is the case, then co-depletion of AIR-1 and SAPS-1 should mimic a phenotype analogous to AIR-1 loss. Indeed, we observed that RNAi-mediated co-depletion of AIR-1 and SAPS-1 [depicted as *air-1 (RNAi); saps-1 (RNAi)*] revealed a phenotype similar to *air-1 (RNAi)* (Fig. 1D; Movie 6), suggesting that

AIR-1 acts downstream of PPH-6. To test the requirement of AIR-1 kinase activity for the observed phenotype, we monitored cortical contractility in embryos expressing an RNAi-resistant form of GFP-AIR-1^R or a kinase-dead mutant (GFP-AIR-1^{R T201A}) upon depletion of endogenous AIR-1 by RNAi. As shown previously, we observed that both GFP-AIR-1^R and GFP-AIR-1^{R T201A} transgenic strains express comparable levels of GFP-tagged proteins (Fig. S1F-H; Toya et al., 2011). Notably, we found that, in contrast to GFP-AIR-1^R embryos, GFP-AIR-1^{R T201A} embryos were unable to rescue the relatively uniform cortical contractility observed upon RNAi-mediated depletion of the endogenous protein (compare Fig. S1K with S1I and J). Overall, these data indicate that SAPS-1 acts upstream of AIR-1, and AIR-1 kinase activity is crucial for proper cortical contractility.

Newly fertilised *C. elegans* one-cell embryos show uniform actomyosin-based cortical contractions that cease at the posterior cortex at the time of polarity establishment (Munro et al., 2004; reviewed by Cowan and Hyman, 2007; Motegi and Seydoux, 2013; Rose and Gönczy, 2014). Therefore, we quantitatively measured cortical contractility in term of membrane ingression in control and *air-1 (RNAi)* embryos expressing the plasma membrane marker GFP-PH (see also figure legends for 1E,F and Materials and Methods for details). In control embryos, cortical ingressions were uniform across the entire embryo surface before the polarity establishment phase, and such ingressions ceased on the posterior cortex at the onset of polarity establishment (Fig. 1E; Movie 7). On the contrary, embryos depleted of AIR-1 show robust cortical ingressions in the posterior cortex that persisted for a prolonged duration and disappeared along with the anterior ingressions at the time of the pronuclear meeting (Fig. 1F; Movie 8).

Next, we examined whether excess contractility upon AIR-1 loss correlates with the change in the cortical localisation of the GFP-NMY-2. Intriguingly, we uncovered that in both control and *air-1 (RNAi)* embryos, GFP-NMY-2 patches appear similar. However, in comparison with control embryos, *air-1 (RNAi)* embryos do not show a stereotypical cortical flow from posterior to anterior, but rather show a weak flow that is directed away from both the poles (Fig. 1G-J, also see Fig. S3; Movies 9 and 10). To characterise cortical flow further, we conducted particle image velocimetry (PIV) analysis in control and *air-1 (RNAi)* embryos in the first 180 s of the GFP-NMY-2 movies (Fig. S1L-O). These analyses indicate that, upon AIR-1 loss, cortical flow is highly reduced at the time of polarity establishment in comparison with control embryos (Fig. S1P). Altogether, these data indicate that relatively uniform ingression-regression on most of the embryo surface upon AIR-1 loss could stem from the weak and non-stereotypical cortical flows.

AIR-1 ensures a single polarity axis in the one-cell embryo

What are the consequences of excess contractility during early cell cycle stages? AIR-1 depletion is implicated in the impairment in the localisation of anterior PAR and posterior PAR (referred as aPAR and pPAR), as well as P granules during late mitotic stages (Schumacher et al., 1998; Noatynska et al., 2010). However, the mechanism by which AIR-1 depletion influences PARs localisation had not been determined. Given that impairment in cortical contractility can affect A-P polarity (Motegi and Sugimoto, 2006; Schonegg and Hyman, 2006; reviewed by Munro, 2006; Cowan and Hyman, 2007), we sought to assess the

impact of AIR-1 loss on pPAR: PAR-2. Notably, in contrast to the control embryos, in which PAR-2 localises at the posterior cell cortex at the initiation of polarity establishment phase, mCherry-PAR-2 signal appeared at the anterior as well as the posterior cell cortex (Fig. 2A-D,H; Movies 11 and 12). Similar data were obtained in a transgenic strain ectopically expressing GFP-PAR-6 and mCherry-PAR-2 (Fig. S2A,B; Movies 13 and 14). In addition, the timing of the appearance of two distinct mCherry-PAR-2 domains in *air-1 (RNAi)* embryos is similar to that in control embryos (Fig. 2E-G).

Furthermore, to evaluate bipolar PAR-2 phenotype in *air-1 (RNAi)* with the cortical flows, we performed time-lapse recording of embryos co-expressing GFP-NMY-2 and mCherry-PAR-2 at the equatorial as well as the cortical plane (Fig. S3; Movies 15-18). As reported previously, control embryos are characterised by segregation of the GFP-NMY-2 from the posterior to the anterior, and this segregation coincides with the mCherry-PAR-2 localisation at the posterior cell cortex (Fig. S3A,C and E; Zonies et al., 2010; Tse et al., 2012). However, as anticipated from the weak flow of GFP-NMY-2 away from the anterior and posterior poles, AIR-1-depleted embryos form two PAR-2 domains (Fig. S3B,D,F).

As another means to check the impact on polarity in *air-1 (RNAi)*, we sought to examine the localisation of P-granule component PGL-1 (Kawasaki et al., 1998) and a germline factor, the PIE-1 protein (Reese et al., 2000). Interestingly, analogous to PAR-2 localisation, GFP-PGL-1 or GFP-PIE-1 are localised at the anterior and posterior of the one-cell embryo in *air-1 (RNAi)*, in contrast to the control embryos, where the signal is restricted to the posterior (Fig. 2I,J; Fig. S2C,D; Movies 19-22). From these data, we conclude that AIR-1 is crucial to ensure single polarity axis.

AIR-1 kinase activity is crucial for proper polarity setup

To characterise the function of AIR-1 kinase activity on polarity establishment, we analysed the establishment of pPAR polarity in the one-cell embryo expressing GFP-AIR-1^R or GFP-AIR-1^{R T201} together with mCherry-PAR-2 upon depletion of endogenous AIR-1. Interestingly, expression of GFP-AIR-1^R, but not kinase-dead GFP-AIR-1^{R T201}, significantly rescued single PAR-2 phenotype, suggesting AIR-1 kinase activity is vital for this phenotype (Fig. S2E,F). Notably, RNAi-mediated depletion of endogenous AIR-1 caused a robust reduction in the levels of GFP-AIR-1^{R T201} at the centrosomes, suggesting that centrosomal localisation of AIR-1 is regulated by its kinase activity (compare Fig. S2F with E).

Centrosome scaffold protein SPD-5 interacts with AIR-1 and localises it to the centrosomes (Hamill et al., 2002; Boxem et al., 2008). SPD-5 depletion is associated with the occurrence of two PAR-2 domains (Tsai and Ahringer, 2007). Therefore, we characterised whether AIR-1 regulates centrosomal levels of SPD-5. Intriguingly, we observed that loss of AIR-1 significantly reduces centrosomal SPD-5 levels (Fig. S2G-J). Because kinase-inactive GFP-AIR-1^{R T201} fails to localise to the centrosome upon depletion of endogenous protein, it appears that AIR-1 kinase activity would be required for SPD-5 recruitment and vice versa. Since SPD-5 plays an essential role in centrosome maturation, and AIR-1 and SPD-5 are dependent on each other for their centrosomal localisation (Hamill et al., 2002; Fig. S2G-J),

at this stage we cannot discriminate whether AIR-1 ensures single posterior PAR-2 axis through its impact on centrosome maturation or directly (see Discussion).

AIR-1 regulates polarity independently of its role in microtubule nucleation

AIR-1 is an essential kinase that is crucial for centrosomal microtubule nucleation and, therefore, bipolar spindle formation (Hannak et al., 2001). As reported earlier, depletion of AIR-1 significantly impairs centrosomal microtubules (Fig. S1A,B,E; Hannak et al., 2001). Because, microtubules are linked with polarity establishment (Wallenfang and Seydoux, 2000; Tsai and Ahringer, 2007; reviewed by Siegrist and Doe, 2007), we sought to investigate whether the decrease in microtubules in *air-1 (RNAi)* could lead to the appearance of two PAR-2 domains. γ -Tubulin depletion by *tbg-1(RNAi)* phenocopies the impact of AIR-1 loss on centrosomal microtubules (Hannak et al., 2001, 2002). We reasoned that if the reduction in microtubules is the causative reason for the occurrence of two PAR-2 domains in *air-1(RNAi)*, then we should mimic this phenotype upon TBG-1 depletion. To this end, we performed *tbg-1 (RNAi)* and observed the loss of GFP signal in GFP-TBG-1 embryos (Fig. S4A,B), highly reduced centrosome asters (Fig. S1C,E) and the collapse of the centrosomes after NEBD (Movie 23). We noticed that the depletion of TBG-1 impacted neither cortical contractility nor PAR-2 localisation (Fig. 3A,B). As a more rigorous test to study the role of microtubules in the context of AIR-1-mediated PAR-2 localisation, we treated AIR-1-depleted early embryos with the microtubule disruptor nocodazole and assessed PAR-2 localisation. Nocodazole treatment further reduces microtubule asters in the *air-1(RNAi)* background but does not entirely abolish centrosomal mCherry-tubulin fluorescence intensity in our experimental setup (Fig. S1D,E; Movie 24). Importantly, nocodazole-treated *air-1 (RNAi)* embryos still harbour two PAR-2 domains (Fig. 3C-E; Movie 25). Altogether, these data suggest that the AIR-1-mediated single PAR-2 axis is independent of its role in regulating centrosomal microtubule asters.

The AIR-1 coactivator TPXL-1 mediates AIR-1 localisation on astral microtubules during mitosis (Özlu et al., 2005). Therefore, we characterised whether TPXL-1 localises AIR-1 onto astral microtubules in the early embryos and, if it does, what impact TPXL-1 depletion has on PAR-2 localisation. *tpxl-1(RNAi)* embryos fail to localise AIR-1 on the astral and cortical microtubules (Fig. S4C,D). Interestingly, *tpxl-1 (RNAi)* embryos neither show excess contractility nor promiscuous PAR-2 domains (Fig. S4E,F; Movie 26). These data, together with the previous results, support the notion that kinase-active AIR-1 that preferentially enriches at the centrosomes (Toya et al., 2011), but not microtubule-associated AIR-1 or its co-activator TPXL-1, is required for ensuring a single polarity axis.

Centrosome position is dispensable for polarity initiation in AIR-1-depleted embryos

In *C. elegans* one-cell embryos, polarity establishment depends on centrosomes (O'Connell et al., 2000; Hamill et al., 2002; Cowan and Hyman, 2004). Moreover, it has been shown that centrosome can initiate polarity from any position within the embryo (Goldstein and Hird, 1996; Bienkowska and Cowan, 2012). However, centrosome-cortex distance defines the polarity establishment timing, i.e. the shorter the distance, the faster the polarity establishment (Bienkowska and Cowan, 2012). Phosphorylated AIR-1 at T201 represents a kinase active form of AIR-1 that primarily accumulates at the centrosomes (Toya et al.,

2011). As AIR-1 kinase activity is essential for ensuring single polarity axis, we decided to establish the contribution of centrosome positioning in modulating pPAR localisation in embryos also depleted for AIR-1. To test this, we used embryos co-expressing GFP-TAC-1 as the centrosomal marker (Bellanger and Gönczy, 2003; Le Bot et al., 2003; Srayko et al., 2003) and mCherry-PAR-2, and examined GFP-TAC-1 position and PAR-2 membrane association during polarity establishment. As expected, we observed that, in control embryos, mCherry-PAR-2 first appears at the cortex in close proximity to the centrosomes (Fig. 4A,G; Movie 27). This was the case even in embryos that underwent lateral fertilisation (Fig. 4B,H; Movie 28). To corroborate this more rigorously, we used the *zyg-12 (RNAi)* condition. ZYG-12 is a member of the Hook family of cytoskeletal linker proteins; loss of ZYG-12 perturbs the attachment of the centrosomes to the nucleus, resulting in untethered centrosomes floating freely in the cytosol (Malone et al., 2003). We observed that, in the *zyg-12 (RNAi)*, movement of centrosomes towards the anterior drives mCherry-PAR-2 at the anterior instead at the posterior cortex (Fig. 4C,I; Movie 29), further strengthening the existing model that centrosome positioning dictates the site for PAR-2 anchoring. Next, we sought to assess mCherry-PAR-2 localisation in AIR-1-depleted embryos where the fertilisation is either lateral or anterior, or centrosomes are not associated with the nucleus because of the loss of ZYG-12. Notably, in all scenarios, PAR-2 localises at the anterior and posterior cortical domains irrespective of the position of the centrosome (Fig. 4D,J;E,K;F,L; Movies 30-32). These results strongly suggest that, in AIR-1 depleted embryos, centrosomes lose the capacity to dictate cortical PAR-2 positioning during polarity establishment in the one-cell embryo.

ECT-2 and its activator NOP-1 act downstream of AIR-1 in regulating polarity establishment

Thus far, our results indicate that active AIR-1 at the centrosome could be the key to initiating the symmetry-breaking event, and thus for polarity establishment at the embryo posterior. In the one-cell embryo, the downregulation of Rho signalling (Fig. 5A) at the posterior cortex at the time of polarity establishment is linked with the membrane exclusion of RhoGEF ECT-2 (Motegi and Sugimoto, 2006). As AIR-1 depletion leads to comparatively uniform ingression-regression and absence of stereotypical cortical flow (Fig. 1; Fig. S3), we wondered whether ECT-2 or its activator NOP-1 (Tse et al., 2012) acts downstream of AIR-1 in controlling cortical contractility. As expected, *air-1 (RNAi); ect-2 (RNAi)* and *air-1 (RNAi); nop-1 (RNAi)* embryos display almost negligible cortical contractility, in contrast to *air-1 (RNAi)* embryos (Fig. 5B-E; Fig. S5A,B). Next, we analysed the impact of ECT-2 or NOP-1 loss on the two PAR-2 domains that occur in *air-1 (RNAi)* condition. Importantly, an additional anterior PAR-2 domain was absent in the majority of *air-1 (RNAi); ect-2 (RNAi)* or *air-1 (RNAi); nop-1 (RNAi)* embryos (Fig. 5F-J; Fig. S5C,D; Movies 33-36). To confirm that the loss of anterior PAR-2 domain in majority of *air-1 (RNAi); ect-2 (RNAi)* embryos was not because of a weak *air-1 (RNAi)* in the double RNAi condition, we fed *C. elegans* with a 1:1 diluted *air-1(RNAi)* feeding bacterial strain. Even with 1:1 dilution, we found a significant number of two PAR-2 domains in the one-cell embryo (Fig. S6A). Moreover, we noticed robust depletion of *air-1* encoding mRNA and protein under such conditions (Fig. S6B-H; also see the efficiency and phenotypes of the double RNAi in Figs S6I-Q and S7A-D). We also observed that the posterior PAR-2 domain appearance was significantly delayed in *ect-2 (RNAi)* or *air-1*

(*RNAi*); *ect-2 (RNAi)* embryos (Fig. 5H,I; Figs S5E and S7C,D). To further corroborate this finding, we relied on *C. elegans* strain coexpressing mCherry-PAR-6 and GFP-PAR-2 in loss-of-function temperature-sensitive *ect-2 (ax751ts)* embryos (Zonies et al., 2010; Tse et al., 2012). RNAi-mediated depletion of AIR-1 in this line significantly suppressed the occurrence of two PAR-2 domains (Fig. 5J; Fig. S7E-H).

Overall, our data suggest that excess contractility at the cell cortex upon *air-1 (RNAi)* drives the formation of two pPAR domains. In addition, the delay in PAR-2 posterior localisation in *ect-2 (RNAi)*; *air-1 (RNAi)* may be dependent on a microtubule-directed pathway that is activated considerably later at the time of polarity maintenance and polarises embryos even in the absence of Rho activation (Zonies et al., 2010; Motegi et al., 2011; Tse et al., 2012).

AIR-1 delocalises ECT-2 at the posterior cortex at the time of polarity establishment

As the loss of ECT-2 localisation at the posterior cortex causes anisotropy in one-cell embryos and establishes polarity (reviewed by Hoegge and Hyman, 2013), we decided to check ECT-2 localisation in embryos depleted of AIR-1. To this end, we used embryos coexpressing GFP-ECT-2 and mCherry-PAR-2, and analysed the cortical localisation of these proteins in the one-cell early embryos. As reported earlier, we noticed the exclusion of GFP-ECT-2 at the posterior cortex in control embryos (Fig. 6A,E,I,J; Motegi and Sugimoto, 2006) and this coincides with the localisation of mCherry-PAR-2 at the posterior cortex (Fig. 6B,F,I,K; Movie 37). Interestingly, in AIR-1-depleted embryos, GFP-ECT-2 remains associated with the posterior cortex, and two mCherry-PAR-2 domains are formed (Fig. 6C,D,G,H,L,M; Movie 38).

The AIR-1-dependent exclusion of GFP-ECT-2 at the posterior cortex could be linked either with the function of AIR-1 in orchestrating microtubule nucleation at the centrosomes or with other effectors that act downstream of AIR-1, or both. TBG-1 (γ -tubulin) and ZYG-9 (an orthologue of XMAP215) centrosomal localisation during mitosis is regulated by AIR-1, and both of these proteins are needed for various aspects of microtubule nucleation (Matthews et al., 1998; Hannak et al., 2001,2002; Srayko et al., 2003; Bellanger and Gönczy, 2003). We found that centrosomal localisation of TBG-1 and ZYG-9 is regulated by AIR-1, even in early embryos (Fig. S8A-F; Movies 39-42). Therefore, we investigated the influence of TBG-1 or ZYG-9 depletion on mCherry-PAR-2 and GFP-ECT-2 cortical localisation. Notably, RNAi-mediated loss of TBG-1 or ZYG-9 does not perturb mCherry-PAR-2 and GFP-ECT-2 localisation (Fig. S9A-I; Movies 43 and 44).

Altogether, our data support the hypothesis that centrosome-localised AIR-1, independently of its function in microtubule nucleation, regulates the formation of a single polarity axis by delocalising ECT-2 from the posterior cortex. These data further indicate that, upon RNAi-mediated depletion of AIR-1, relatively uniform cortical contractility driven by non-exclusion of the RhoGEF ECT-2 from the posterior cortex causes the formation of multiple polarity axes.

Discussion

The proper establishment of polarity axis during various stages of development is vital for regulating multiple events such as cell division, cell migration and cell signalling. Across numerous cell types, distinct signals trigger polarity establishment. For example, epithelial cells polarise in response to the extrinsic cues from their neighbours, mating yeast cells polarise in response to the signals from each other and *C. elegans* one-cell stage embryos polarise following sperm entry immediately after fertilisation (reviewed by Chant, 1999; Nelson, 2003; Pellettieri and Seydoux, 2002; St Johnston, 2018). In the one-cell *C. elegans* embryo, the cortical actomyosin network is considered to act as a significant driving force for the asymmetric distribution of the molecules that are responsible for the polarity establishment (Munro et al., 2004; reviewed by Munro and Bowerman, 2009). In this study, we demonstrate a novel function of AIR-1 in modulating actomyosin network through RhoGEF ECT-2, and uncover that this action of AIR-1 is crucial for ensuring the establishment of single polarity axis in the *C. elegans* one-cell embryo.

AIR-1 is crucial for regulating proper cortical contractility and polarity establishment

Our results demonstrate that severe depletion of AIR-1 causes pronounced cortical contractions at the time of polarity setup, which leads to the appearance of two PAR-2 domains (Fig. 7). The impact of AIR-1 loss on cortical contractility is antagonistic to the loss of PP6 phosphatase regulatory subunit SAPS-1. Furthermore, by conducting epistasis experiments, we revealed that AIR-1 acts downstream of SAPS-1. In human cells, PP6 acts as a major T-loop phosphatase for Aurora A (Zeng et al., 2010), and thus it may well be that the analogous situation exists in *C. elegans* embryos in which the PPH-6/SAPS-1 phosphatase complex buffers AIR-1 activity to modulate proper cortical contractility. Notably, in the line of this hypothesis, we uncovered that AIR-1 kinase activity is crucial for this function. Interestingly, we found that TPXL-1, a coactivator of AIR-1, which is also required to localise AIR-1 to the microtubules, is not essential for AIR-1-mediated cortical contractility.

A centrosome scaffold protein SPD-5 is required for AIR-1 enrichment at the centrosomes, and we show that AIR-1, in turn, is needed for SPD-5 localisation at the centrosomes (Hamill et al., 2002; Fig. S2G-J). SPD-5 is further necessary for centrosomes maturation (Hamill et al., 2002; Woodruff et al., 2017). Importantly, SPD-5 depletion is associated with the occurrence of two PAR-2 domains (Tsai and Ahringer, 2007), and thus one possibility could be that loss of AIR-1 impacts centrosomes maturation by influencing centrosomal SPD-5 levels and this leads to bipolar PAR-2 domain formation. At this stage, our data do not exclude the role of AIR-1 role in regulating a single PAR-2 axis is through its function in maintaining SPD-5 at the centrosome, and thus addressing this important issue will be of interest for future investigations. Nonetheless, based on the finding that polarisation is faster if the centrosome to the cell cortex distance is shorter (Bienkowska and Cowan, 2012), and on the recent studies revealing that centrosomal AIR-1 is highly dynamic in contrast to SPD-5 in the FRAP analysis (Kress et al., 2013; Laos et al., 2015), we favour the model that AIR-1, independently of its role in centrosome maturation, plays a vital function in proper polarity establishment.

How does AIR-1 influence cortical contractility and polarity establishment in the one-cell embryo? As phosphorylated AIR-1 at T201 is predominantly localised to the centrosome (Toya et al., 2011), and its kinase activity seems to be crucial for preventing excess contractility and multiple polarity axes, we propose that, in wild-type embryos, there might be a gradient of active AIR-1 emanating from the centrosome that could be the key to assisting symmetry breaking in the vicinity of centrosome by initiating the anterior directed cortical flow (Fig. 7). Such robust flows possibly concentrate anterior PARs at the anterior pole to prevent ectopic PAR-2 formation.

In agreement with this hypothesis, we uncovered that AIR-1 depletion at the time of polarity establishment fails to clear ECT-2 from the posterior cell cortex close to the nuclear-centrosome complex, and possibly this promotes the formation of spontaneous pPAR domains on the anterior as well as the posterior cell cortex (Fig. 7). However, as centrosomal AIR-1 rapidly exchanges with the cytoplasmic pool (Kress et al., 2013), our experiments cannot entirely rule out the contribution of the cytoplasmic pool away from the centrosome in preventing excess contractility and promiscuous PAR-2 domains. Future work using optogenetics to temporally target ECT-2 to the entire membrane, or restricting AIR-1 only to the centrosomes would be crucial in providing further in-depth mechanistic insights of the polarity establishment pathway.

ECT-2: an evolutionarily conserved RhoGEF at the front line of proper polarity setup

ECT-2 is an evolutionarily conserved RhoGEF that plays a vital role in polarity establishment (Liu et al., 2004; Motegi and Sugimoto, 2006; Liu et al., 2006; Rosa et al., 2015), cell rounding (Matthews et al., 2012) and in the formation of the cleavage furrow (Prokopenko et al., 1999; Tatsumoto et al., 1999; Dechant and Glotzer, 2003; Yüce et al., 2005). In mammalian cells, the C-terminal of Ect2 possesses PH and PBC domains that are responsible for its interaction with membrane phosphoinositides (Chalamalasetty et al., 2006; Su et al., 2011). The ectopic localisation of Ect2 at the plasma membrane is associated with excess membrane ruffling at the time of furrow formation by regulating cortical actomyosin activity (Su et al., 2011). Our data reveal that in *C. elegans* one-cell embryos, ECT-2 decorates the entire embryo surface upon AIR-1 depletion. Thus, one possibility is that during polarity establishment, ECT-2 relies on phosphoinositide-based membrane lipids for its localisation, and AIR-1 directly or indirectly helps in changing the lipid-binding behaviour of ECT-2 and therefore helps in breaking the symmetry. Further work based on biochemical kinase assays using AIR-1 and ECT-2 in combination with lipid-binding studies will be required to test whether ECT-2 is a direct target of AIR-1; if it is, it would be equally crucial to examine the influence of such AIR-1 mediated phosphorylation on ECT-2 lipid-binding potential in this paradigm.

The microtubule nucleation function of AIR-1 is not crucial for accurate polarity setup

The role of microtubules in the anterior-posterior axis formation is well documented in several model organisms, including in the *C. elegans* one-cell embryo (Tsai and Ahringer, 2007; Wallenfang and Seydoux, 2000; reviewed by Siegrist and Doe, 2007). Keeping this in mind, we have tested whether AIR-1 influences polarity establishment via its proposed function related to microtubule nucleation (Hannak et al., 2001). Embryos depleted of

TBG-1 show an impairment of microtubule nucleation to a similar extent as upon AIR-1 loss. However, *tbg-1(RNAi)* embryos show neither excess contractility nor polarity establishment defects, suggesting that the role of AIR-1 in maintaining a single pPAR axis is not through its contribution to microtubules nucleation. In this realm, ZYG-9, a protein that localises to the centrosomes in an AIR-1-dependent manner and is required to ensure the correct length of microtubules (Srayko et al., 2003), is not necessary for ECT-2 delocalisation or for PAR-2 localisation. Altogether, these observations suggest that the role of AIR-1 in maintaining the proper number of centrosomal microtubules is not key to its function in polarity establishment.

AIR-1 ensures a single pPAR axis

RNAi-mediated depletion of AIR-1 leads to the formation of two pPAR axes at the time of polarity setup. This outcome was somewhat surprising. If the centrosome-enriched pool of AIR-1 is a positive regulator of anisotropy and thereby creates single PAR-2 in the wild-type embryos, then should the loss of AIR-1 not establish pPAR polarity at all? As the appearance of the two pPAR axes can be rescued by simultaneous depletion of AIR-1 with ECT-2 or NOP-1, it is likely that the cortical contractions on the entire embryo surface in *air-1 (RNAi)* are mediating the formation of two PAR-2 domains. In such co-depleted embryos, we expect to see the loss of PAR-2 localisation at the cell cortex during polarity establishment. Indeed, co-depletion of AIR-1 and ECT-2 abolishes timely PAR-2 localisation, and PAR-2 only appears at the posterior cortex at the time of the pronuclear meeting, possibly via a microtubule-dependent pathway (Fig. 7; Motegi et al., 2011; Tse et al., 2012).

Another reason for the existence of two pPAR axes in *air-1(RNAi)* embryos could be that, in the wild-type embryos, PAR-2 is usually cleared from the anterior cortex in AIR-1-dependent manner; thus, loss of AIR-1 leads to an ectopic anterior PAR-2. This assumption aligns with studies where mutants arrested in meiosis can guide the formation of PAR-2 domain at the anterior cortex (Wallenfang and Seydoux, 2000; Tsai and Ahringer, 2007). However, this notion appears to be unlikely as: (1) we did not observe any significant change in the timing of meiosis completion upon AIR-1 depletion (Schumacher et al., 1998; data not shown); (2) in *air-1(RNAi); zyg-12(RNAi)* embryos where centrosomes are uncoupled from the nuclear envelope and are much closer to the anterior cortex, two pPAR domains are present; (3) in the *air-1(RNAi)* condition, few embryos that undergo anterior fertilisation still show the formation of two PAR-2 domains; (4) phosphorylated AIR-1 at T201 mainly accumulates at the centrosomes, and AIR-1 activity appears to be crucial for preventing two PAR-2 domains; and (5) removal of contractility-associated genes rescues the bipolar phenotype in an *air-1(RNAi)* background. Based on the reasons mentioned above, we envisage that the promiscuous PAR-2 domain that arises after AIR-1 loss is not related to the function of AIR-1 in clearing PAR-2 at the anterior cortex.

It is pertinent that the appearance of two PAR-2 domains in *air-1(RNAi)* are invariably and primarily restricted to only the anterior and posterior polar cortical regions. As the cell cortex is characterised by the visco-elastic properties modulated by the dynamic nodes of myosin interacting with the underlying actin network (Munro et al., 2004; reviewed by

Hoege and Hyman, 2013), it is possible that, because of the presence of curvature at the very anterior and posterior domain of the embryo, these nodes are less connected in comparison with the rest of embryo and thus such locations are more amenable for symmetry breaking. In the future, it will be interesting to dissect whether the physical basis of the embryo shape is at play to break symmetry in the *air-1* (*RNAi*) background.

Overall, our study sheds light on a long-standing puzzle by showing that AIR-1 acts as the polarising signal at the centrosome that initiates polarity establishment via its impact on actomyosin-based cortical contractility. Additionally, while our paper was in revision, studies published by Klinkert and colleagues (2019), Zhao and colleagues (2019), and Reich and colleagues (2019) support our proposed model for the crucial role of Aurora A in regulating proper polarity establishment. Moreover, as Aurora A is an evolutionarily conserved gene, it is probable that the function of Aurora A on actomyosin-mediated cortical contractions is a general paradigm that is relevant to various biological processes beyond polarity establishment.

Materials and Methods

C. elegans strains and drug treatment

C. elegans wild type (N2) as well as transgenic lines expressing endogenously tagged mCherry-PAR-2 (KK1254); RNAi-resistant GFP-AIR-1^R or a kinase-dead mutant equivalent (GFP-AIR-1^R T201A) (Toya et al., 2011); GFP-NMY-2 (Munro et al., 2004); GFP-PH (Audhya et al., 2005); GFP-PAR-2; mCherry-PAR-6 (GZ869); GFP-TAC-1 (Bellanger and Gonczy, 2003); GFP-ECT-2 (Motegi and Sugimoto, 2006); GFP-PIE-1 (JH2015); GFP-PGL-1 (SS747); GFP-TBG-1 (TH27); mCherry-ZYG-9 (TH165); GFP-SPD-5 (DAM309); mCherry-tubulin (JA1559); mCherry-PAR-6, GFP-PAR-2 in *ect-2(ax751ts)* (JH2657); mCherry-PAR-2, GFP-TAC-1 (SK001; this study); mCherry-PAR-2, GFP-ECT-2 (SK002; this study); mCherry-PAR-2, GFP-AIR-1 (SK003; this study); mCherry-PAR-2, GFP-tubulin (SK004; this study); mCherry-PAR-2, GFP-AIR-1R (SK005; this study); mCherry-PAR-2, GFP-AIR-1^R T201A (SK006; this study); and mCherry-PAR-2, GFP-NMY-2 (SK007) were maintained at 24°C.

Microtubule poisoning with nocodazole was performed as described previously (Bienkowska and Cowan, 2012). In brief, worms were dissected in nocodazole (10 µg/ml; Sigma Aldrich, M1404) containing egg buffer [118 mM NaCl, 40 mM KCl, 3.4 mM MgCl₂, 3.4 mM CaCl₂ and 5 mM HEPES (pH 7.4); also see Boyd et al., 1996] and drug could enter in the embryos because of the permeability of the eggshell during meiosis II (Johnston et al., 2006). The efficiency of nocodazole was determined by the inability of the pronuclei to migrate and by the impact on the centrosomal mCherry-tubulin fluorescence intensity (see Fig. S1 and Movie 24).

RNAi experiments

Bacterial RNAi feeding strains for *saps-1*, *air-1*, *ect-2*, *nop-1*, *tbg-1* and *zyg-12* were obtained either from the *C. elegans* ORFeome RNAi library or from Source BioScience (Kamath et al., 2003). The *tpxl-1* (*RNAi*) construct has been described previously (Özlu et

al., 2005) as the *air-1^N(RNAi)* feeding strain (Toya et al., 2011; Kotak et al., 2016). RNAi against *saps-1*, *air-1*, *air-1^S* (targeting 1-564 bp of *air-1* gene), *air-1*; *saps-1*, *tbg-1*, *tpx1-1*, *zyg-12*, *ect-2*, *air-1*; *ect-2*, *air-1*; *nop-1*, *air-1*; *zyg-12* and *air-1*; *nos-1* was performed by feeding animals starting at the L2 or L3 stage with bacteria expressing the corresponding dsRNAs at 20°C or 24°C for 24-40 h before analysis. While performing double depletion using RNAi, the single depletion was performed side by side to observe the single RNAi-mediated phenotype. In addition, for assessing the efficiency of double depletion, e.g. in the case of *air-1 (RNAi) ect-2 (RNAi)*, beyond relying solely on the phenotype, we also checked the depletion efficiency by using *C. elegans* strains expressing mCherry-PAR-2; GFP-ECT-2 or mCherry-PAR-2; GFP-AIR-1 to make sure that we efficiently lost GFP signal in these transgenic strains. We also observed highly reduced centrosomal intensity and centrosomal collapsing after NEBD in a *C. elegans* strain expressing mCherry-PAR-2; GFP-tubulin (see also Fig. S5 and associated legend). In addition, in cases where RNAi-mediated double depletion masks the phenotype(s) of any individual RNAi, as in *saps-1 (RNAi) air-1 (RNAi)*, where the phenotype stem from the AIR-1 loss masks the *saps-1 (RNAi)* phenotype, the standardisation was carried out by conducting immunostaining analysis using SAPS-1 antibodies to validate the efficient depletion (data not shown).

air-1(RNAi) experiments using mCherry-PAR-6; GFP-PAR-2 in *ect-2(ax751ts)* [JH2657] were performed by picking L3-L4 on RNAi feeding plate for 12 h at 15°C followed by shifting the feeding plates to the restrictive temperature of 24°C for 24 h.

Time-lapse microscopy

For most experiments, gravid worms were dissected in M9 or egg buffer and transferred onto a 2% agarose pad containing slides using a mouth pipette. These were then covered with a 20×20 mm coverslip. Time-lapse differential interference contrast (DIC) microscopy, dual DIC and confocal microscopy or DIC in combination with fluorescence microscopy were performed on such embryos either on IX53 (Olympus) with Qimaging Micropublisher 5.0 Colour CCD Camera (Qimaging) with 100×1.4 NA, FV3000 confocal system with a high-sensitivity cooled GaAsP detection unit (Olympus) using a 60×1.4 NA objective or on IX83 with XM10 cool CCD chip camera (Olympus) using a 60×1.4 NA objective. Images were collected at 5-20 s intervals. Movies were subsequently processed using ImageJ, QuickTime and Adobe Photoshop, maintaining relative image intensities within a series. Z-stack series were projected as maximum intensity projections for embryos expressing GFP-TAC-1, mCherry-tubulin and GFP-AIR-1.

Indirect immunofluorescence

Embryo fixation and staining for indirect immunofluorescence was performed mostly as described (Gönczy et al., 1999), using 1:200 mouse anti- α -tubulin antibodies (DM1A, Sigma), in combination with 1:200 rabbit anti-AIR-1 (Hannak et al., 2001). Embryos were fixed in methanol at -20°C for 30 min and incubated with primary antibodies for 1 h at room temperature. Secondary antibodies were Alexa488-coupled anti-mouse (ThermoFisher, A11001) and Alexa568-coupled anti-rabbit (ThermoFisher, A11011), both used at 1:500. Confocal images were acquired on a FV3000 confocal system with high-sensitivity cooled

GaAsP detection unit (Olympus) using a 60× objective with NA 1.4 oil and processed in ImageJ and Adobe Photoshop, maintaining relative image intensities.

Quantitative RT-PCR analysis

Total RNA was isolated from the eggs of adult worms of N2 from mock and RNAi feeding plates, using a Qiagen Universal RNA isolation kit. Genomic contamination was removed using Thermo Scientific DNase1 (EN0521), following which cDNA was generated using Revertaid reverse transcriptase (Thermo Fisher Scientific, EP0441). RT-qPCR was performed using dsDNA dye TB Green Premix Ex Taq II (Takara Bio, RR820A) on a BioRad CFX96 real-time PCR machine. The Delta Ct method was used for calculation of relative mRNA levels. Relative quantitation of mRNA level was determined by standardising against T04C12.6 (*act-1*). The values obtained were normalised to control N2 mRNA levels. Statistical analysis was carried out using one-way ANOVA and Tukey's multiple comparison test (GraphPad Version 8).

Data analysis

Fiji (fiji.sc/), GraphPad Prism and MATLAB (MathWorks) were used to perform quantitative analysis. Kymograph analysis of embryos expressing GFP-NMY-2 was performed as described earlier (Munro et al., 2004). In brief, an 8-pixel thick section was extracted roughly from the centre of each image from a time-lapse sequence, and thereafter, stacked vertically using MATLAB, to generate 2-D kymograph images, with *y*-axis corresponding to time. The speeds were computed from the local slope of kymograph trajectories. The trajectories selected for analysis were manually drawn and were visible in at least five consecutive frames. Width and height of the trajectories, used for calculating the slope, were determined using Fiji. More than ten trajectories drawn over five embryos in control and *air-1 (RNAi)* were used for analysis. Speeds were compared using two-tailed unpaired *t*-test in GraphPad Prism.

A laplace edge detection filter (Cell Dimension Software, Olympus) was applied to time-lapse movies of GFP-PH embryos, in Fig. 1E,F. For the quantification of cortical contractility, the cortical region of the embryo was divided roughly in 60% anterior and 40% posterior halves, and the number of ingressions in both halves were manually counted in each frame of a time-lapse sequence and plotted over time.

For mCherry-PAR-2 and GFP-ECT-2 kymographs, a 50-pixel thick section of the cortex was manually tracked and straightened on Fiji. Resulting images of the time-lapse series were stacked vertically using MATLAB, to generate 2-D kymographs, with the *y*-axis corresponding to time. For the cortical line scans, in Fig. 6J-M, the intensity profile (seven pixels) along the cortex was determined using Fiji, and the values were plotted in Excel.

Assigning time '0' for embryos expressing GFP-NMY-2 and GFP-PH

For GFP-NMY-2 cortical imaging and GFP-PH imaging, $t=0$ corresponding to the frame from where the imaging was initiated, i.e. approximately at the time of polarity establishment just a few minutes after meiosis II completion.

Assigning time '0' for embryos expressing the fluorescently tagged PAR-2 protein

Previously, it has been reported that at the time of completion of female meiosis, the size of the male pronucleus is 3 μm (Bienkowska and Cowan, 2012). In our time-lapse recordings, we uncovered that the size of the male pronucleus is around 5-6 μm at the time of posterior smoothening or symmetry breaking (referred to as polarity establishment). As male and female pronuclei are next to the posterior and anterior cortex at this time, their position is also considered as a proxy for assigning the timing of the polarity establishment. Because of the lack of cortical flow in embryos depleted of ECT-2 or NOP-1, either alone or in combination with AIR-1, the polarity establishment phase (time '0') is determined only by the size of the pronucleus (5-6 μm). For assigning time '0' in DIC recordings, we analysed the appearance of the non-contractile posterior domain and also checked the diameter of the male pronucleus, which is never beyond 5-6 μm at this point of time.

Assigning time '0' for embryos expressing GFP-PIE-1

For assigning time '0' in GFP-PIE-1-expressing worms, we analysed the appearance of the non-contractile posterior domain and also checked the diameter of the male pronucleus, which is never more than 5-6 μm at this time.

Particle image velocimetry analysis

Particle image velocimetry (PIV) analysis of NMY-2 cortical flow was performed on maximum intensity projections of sequential time-lapse images from GFP-NMY-2 recordings, using a freely available PIV algorithm, PIVlab 1.32 (pivlab.blogspot.com/). A 171 \times 85 pixel (35.42 \times 17.61 μm) region of interest was applied to standardise the cortex area excluding the edges of the embryo. Single-pass PIV with interrogation area of 24 \times 12 pixels with 50% overlap was applied, as described by Nishikawa et al. (2017). Under the available post-processing options, vector validation was carried out by setting the threshold to s.d.=7, and data smoothening was performed. Obtained values of the velocity field were plotted using a custom-written MATLAB program, with the help of MATLAB functions obtained from Ronen Zaidel-Bar's laboratory (celladhesionlab.com/).

Quantification of centrosome fluorescence intensity

A fixed circular region of interest (ROI) was placed manually on the centrosome at the time of the pronuclei meeting in maximum intensity z -projections of GFP-AIR-1^R, GFP-AIR-1^R T201A, GFP-TBG-1, ZYG-9-mCherry and GFP-SPD-5. The integrated fluorescence intensity in this ROI and a similarly sized ROI in the cytoplasm and background was determined using Fiji/ImageJ. Fluorescence intensity at the centrosome and cytoplasm was subtracted from the background, and the ratio of centrosome/cytoplasm was used for plotting the graph. Signal intensities were compared using two-sample t -test in GraphPad Prism.

Quantification of centrosome diameter in GFP-SPD-5-expressing embryos

Centrosome intensity profile across a line of 1 μm thickness, at the time of the pronuclei meeting in maximum z projections of GFP-SPD-5, was carried out using Fiji (for generating intensity profiles, longest axis across the centrosome was visually identified.) FWHM (full

width at half maxima) was determined using a Gaussian curve fitted to the intensity profile values, using OriginLab. FWHM was taken as a measure of centrosome diameter (Greenan et al., 2010). FWHM values were compared using two-tailed unpaired *t*-test in GraphPad Prism.

Supplementary Material

Refer to Web version on PubMed Central for supplementary material.

Acknowledgements

We thank Asako Sugimoto, Pierre Gönczy, Nathan Goehring, Subramaniam K, Fumio Motegi, Masanori Mishima, Michael Glotzer and Anthony Hyman for sharing their precious reagents with us. We also thank the Caenorhabditis Genetics Center (CGC) for providing us with all the required worm strains. We are grateful to Daniel St Johnston, Nathan Goehring, Mark Petronczki, Sveta Chakrabarti, Phong Tran, Subramaniam K and Raj Ladher for critical comments on the manuscript. We are thankful to Pierre Gönczy for allowing us to conduct some initial DIC work in his lab, and to Coralie Busso for her help in swiftly arranging all the reagents for shipment during the establishment of the Kotak lab and thereafter. We further thank Sveta Chakrabarti for her help with quantitative RT-PCR analysis. We greatly appreciate help from Prerna Sharma and Debasmita Mondal [Department of Physics, Indian Institute of Science (IISc)] in particle image velocimetry (PIV) analysis of GFP-NMY-2 movies. We thank Ong Hui Ting and Ronen Zaidel-Bar (Sackler Faculty of Medicine, Tel Aviv) for providing us with the Matlab code for PIV analysis. We thank DST-FIST, the UGC Centre for the Advanced Study, the DBT-IISc Partnership Program and the IISc for the infrastructure support.

Funding

This work is supported by the Department of Biotechnology (DBT)-Indian Institute of Science Partnership Program and by grants from the Wellcome Trust/DBT India Alliance Fellowship (IA/I/15/2/502077 to S. Kotak). S. Kotak is a Wellcome Trust DBT-India Alliance Intermediate Fellow.

References

- Afshar K, Werner ME, Tse YC, Glotzer M, Gönczy P. Regulation of cortical contractility and spindle positioning by the protein phosphatase 6 PPH-6 in one-cell stage *C. elegans* embryos. *Development*. 2010; 137:237–247. DOI: 10.1242/dev.042754 [PubMed: 20040490]
- Audhya A, Hyndman F, McLeod IX, Maddox AS, Yates JR III, Desai A, Oegema K. A complex containing the Sm protein CAR-1 and the RNA helicase CGH-1 is required for embryonic cytokinesis in *Caenorhabditis elegans*. *J Cell Biol*. 2005; 171:267–279. DOI: 10.1083/jcb.200506124
- Bellanger J-M, Gönczy P. TAC-1 and ZYG-9 form a complex that promotes microtubule assembly in *C. elegans* embryos. *Curr Biol*. 2003; 13:1488–1498. DOI: 10.1016/S0960-9822(03)00582-7
- Bienkowska D, Cowan CR. Centrosomes can initiate a polarity axis from any position within one-cell *C. elegans* embryos. *Curr Biol*. 2012; 22:583–589. DOI: 10.1016/j.cub.2012.01.64 [PubMed: 22425158]
- Boxem M, Maliga Z, Klitgord N, Li N, Lemmens I, Mana M, de Lichtervelde L, Mul JD, van de Peut D, Devos M, et al. A protein domain-based interactome network for *C. elegans* early embryogenesis. *Cell*. 2008; 134:534–545. DOI: 10.1016/j.cell.2008.07.009 [PubMed: 18692475]
- Boyd L, Guo S, Levitan D, Stinchcomb DT, Kempfues KJ. PAR-2 is asymmetrically distributed and promotes association of P granules and PAR-1 with the cortex in *C. elegans* embryos. *Development*. 1996; 122:3075–3084. [PubMed: 8898221]
- Chalamalasetty RB, Hummer S, Nigg EA, Sillje HHW. Influence of human Ect2 depletion and overexpression on cleavage furrow formation and abscission. *J Cell Sci*. 2006; 119:3008–3019. DOI: 10.1242/jcs.03032 [PubMed: 16803869]
- Chant J. Cell polarity in yeast. *Annu Rev Cell Dev Biol*. 1999; 15:365–391. DOI: 10.1146/annurev.cellbio.15.1.365 [PubMed: 10611966]

- Cowan CR, Hyman AA. Centrosomes direct cell polarity independently of microtubule assembly in *C. elegans* embryos. *Nature*. 2004; 431:92–96. DOI: 10.1038/nature02825 [PubMed: 15343338]
- Cowan CR, Hyman AA. Acto-myosin reorganization and PAR polarity in *C. elegans*. *Development*. 2007; 134:1035–1043. DOI: 10.1242/dev.000513 [PubMed: 17287245]
- Cuenca AA, Schetter A, Aceto D, Kempfues K, Seydoux G. Polarization of the *C. elegans* zygote proceeds via distinct establishment and maintenance phases. *Development*. 2003; 130:1255–1265. DOI: 10.1242/dev.00284 [PubMed: 12588843]
- Dechant R, Glotzer M. Centrosome separation and central spindle assembly act in redundant pathways that regulate microtubule density and trigger cleavage furrow formation. *Dev Cell*. 2003; 4:333–344. DOI: 10.1016/S1534-5807(03)00057-1 [PubMed: 12636915]
- Fortin SM, Marshall SL, Jaeger EC, Greene PE, Brady LK, Isaac RE, Schrandt JC, Brooks DR, Lyczak R. The PAM-1 aminopeptidase regulates centrosome positioning to ensure anterior-posterior axis specification in one-cell *C. elegans* embryos. *Dev Biol*. 2010; 344:992–1000. DOI: 10.1016/j.ydbio.2010.06.016 [PubMed: 20599902]
- Giet R, McLean D, Descamps S, Lee MJ, Raff JW, Prigent C, Glover DM. *Drosophila* Aurora A kinase is required to localize D-TACC to centrosomes and to regulate astral microtubules. *J Cell Biol*. 2002; 156:437–451. DOI: 10.1083/jcb.200108135 [PubMed: 11827981]
- Goehring NW, Trong PK, Bois JS, Chowdhury D, Nicola EM, Hyman AA, Grill SW. Polarization of PAR proteins by advective triggering of a pattern-forming system. *Science*. 2011; 334:1137–1142. DOI: 10.1126/science.1208619 [PubMed: 22021673]
- Goldstein B, Hird SN. Specification of the anteroposterior axis in the *Caenorhabditis elegans* embryo. *Development*. 1996; 122:1467–1474. [PubMed: 8625834]
- Gönczy P, Schnabel H, Kaletta T, Amores AD, Hyman T, Schnabel R. Dissection of cell division processes in the one cell stage *Caenorhabditis elegans* embryo by mutational analysis. *J Cell Biol*. 1999; 144:927–946. DOI: 10.1083/jcb.144.5.927 [PubMed: 10085292]
- Greenan G, Brangwynne CP, Jaensch S, Gharakhani J, Jülicher F, Hyman AA. Centrosome size sets mitotic spindle length in *Caenorhabditis elegans* embryos. *Curr Biol*. 2010; 20:353–358. DOI: 10.1016/j.cub.2009.12.050 [PubMed: 20137951]
- Guo S, Kempfues KJ. A non-muscle myosin required for embryonic polarity in *Caenorhabditis elegans*. *Nature*. 1996; 382:455–458. DOI: 10.1038/382455a0 [PubMed: 8684486]
- Hachet V, Canard C, Gönczy P. Centrosomes promote timely mitotic entry in *C. elegans* embryos. *Dev Cell*. 2007; 12:531–541. DOI: 10.1016/j.devcel.2007.02.015 [PubMed: 17419992]
- Hamill DR, Severson AF, Carter JC, Bowerman B. Centrosome Maturation and mitotic spindle assembly in *C. elegans* Require SPD-5, a protein with multiple coiled-coil Domains. *Dev Cell*. 2002; 3:673–684. DOI: 10.1016/S1534-5807(02)00327-1 [PubMed: 12431374]
- Hannak E, Kirkham M, Hyman AA, Oegema K. Aurora-A kinase is required for centrosome maturation in *Caenorhabditis elegans*. *J Cell Biol*. 2001; 155:1109–1116. DOI: 10.1083/jcb.200108051
- Hannak E, Oegema K, Kirkham M, Gönczy P, Habermann B, Hyman AA. The kinetically dominant assembly pathway for centrosomal asters in *Caenorhabditis elegans* is gamma-tubulin dependent. *J Cell Biol*. 2002; 157:591–602. DOI: 10.1083/jcb.200202047 [PubMed: 12011109]
- Hill DP, Strome S. Brief cytochalasin-induced disruption of microfilaments during a critical interval in 1-cell *C. elegans* embryos alters the partitioning of developmental instructions to the 2-cell embryo. *Development*. 1990; 108:159–172. [PubMed: 2190787]
- Hoeg C, Hyman AA. Principles of PAR polarity in *Caenorhabditis elegans* embryos. *Nat Rev Mol Cell Biol*. 2013; 14:315–322. DOI: 10.1038/nrm3558 [PubMed: 23594951]
- Johnston WL, Krizus A, Dennis JW. The eggshell is required for meiotic fidelity, polar-body extrusion and polarization of the *C. elegans* embryo. *BMC Biol*. 2006; 4:35. doi: 10.1186/1741-7007-4-35 [PubMed: 17042944]
- Kamath RS, Fraser AG, Dong Y, Poulin G, Durbin R, Gotta M, Kanapin A, Le Bot N, Moreno S, Sohrmann M, et al. Systematic functional analysis of the *Caenorhabditis elegans* genome using RNAi. *Nature*. 2003; 421:231–237. DOI: 10.1038/nature01278 [PubMed: 12529635]

- Kawasaki I, Shim Y-H, Kirchner J, Kaminker J, Wood WB, Strome S. PGL-1, a predicted RNA-binding component of germ granules, is essential for fertility in *C. elegans*. *Cell*. 1998; 94:635–645. DOI: 10.1016/S0092-8674(00)81605-0 [PubMed: 9741628]
- Klinkert K, Levernier N, Gross P, Gentili C, von Tobel L, Pierron M, Busso C, Herrman S, Grill SW, Kruse K, et al. Aurora A depletion reveals centrosome-independent polarization mechanism in *Caenorhabditis elegans*. *eLife*. 2019; 8:e44552. doi: 10.7554/eLife.44552 [PubMed: 30801250]
- Kotak S, Afshar K, Busso C, Gönczy P. AuroraAkinase regulates proper spindle positioning in *C. elegans* and in human cells. *J Cell Sci*. 2016; 129:3015–3025. DOI: 10.1242/jcs.184416 [PubMed: 27335426]
- Kress E, Schwager F, Holtackers R, Seiler J, Prodon F, Zanin E, Eiteneuer A, Toya M, Sugimoto A, Meyer H, et al. The UBXLN-2/p37/p47 adaptors of CDC-48/p97 regulate mitosis by limiting the centrosomal recruitment of Aurora A. *J Cell Biol*. 2013; 201:559–575. DOI: 10.1083/jcb.201209107 [PubMed: 23649807]
- Laos T, Cabral G, Dammermann A. Isotropic incorporation of SPD-5 underlies centrosome assembly in *C. elegans*. *Curr Biol*. 2005; 25:R648–R649. DOI: 10.1016/j.cub.2015.05.060
- Le Bot N, Tsai M-C, Andrews RK, Ahringer J. TAC-1, a regulator of microtubule length in the *C. elegans* embryo. *Curr Biol*. 2003; 13:1499–1505. DOI: 10.1016/S0960-9822(03)00577-3 [PubMed: 12956951]
- Littlepage LE, Wu H, Andresson T, Deanehan JK, Amundadottir LT, Ruderman JV. Identification of phosphorylated residues that affect the activity of the mitotic kinase Aurora-A. *Proc Natl Acad Sci USA*. 2002; 99:15440–15445. DOI: 10.1073/pnas.202606599 [PubMed: 12422018]
- Liu X-F, Ishida H, Raziuddin R, Miki T. Nucleotide exchange factor ECT2 interacts with the polarity protein complex Par6/Par3/protein kinase C ζ and regulates PKC ζ activity. *Mol Cell Biol*. 2004; 24:6665–6675. DOI: 10.1128/MCB.24.15.6665-6675.2004 [PubMed: 15254234]
- Liu XF, Ohno S, Miki T. Nucleotide exchange factor ECT2 regulates epithelial cell polarity. *Cell Signal*. 2006; 18:1604–1615. DOI: 10.1016/j.cellsig.2006.01.007 [PubMed: 16495035]
- Malone CJ, Misner L, Le Bot N, Tsai M-C, Campbell JM, Ahringer J, White JG. The *C. elegans* hook protein, ZYG-12, mediates the essential attachment between the centrosome and nucleus. *Cell*. 2003; 115:825–836. DOI: 10.1016/S0092-8674(03)00985-1 [PubMed: 14697201]
- Mangal S, Sacher J, Kim T, Osório DS, Motegi F, Carvalho AX, Oegema K, Zanin E. TPXL-1 activates Aurora A to clear contractile ring components from the polar cortex during cytokinesis. *J Cell Biol*. 2018; 217:837–848. DOI: 10.1083/jcb.201706021 [PubMed: 29311228]
- Matthews LR, Carter P, Thierry-Mieg D, Kemphues K. ZYG-9, a *Caenorhabditis elegans* protein required for microtubule organization and function, is a component of meiotic and mitotic spindle poles. *J Cell Biol*. 1998; 141:1159–1168. DOI: 10.1083/jcb.141.5.1159 [PubMed: 9606208]
- Matthews HK, Delabre U, Rohn JL, Guck J, Kunda P, Baum B. Changes in Ect2 localization couple actomyosin-dependent cell shape changes to mitotic progression. *Dev Cell*. 2012; 23:371–383. DOI: 10.1016/j.devcel.2012.06.003 [PubMed: 22898780]
- Motegi F, Seydoux G. The PAR network: redundancy and robustness in a symmetry-breaking system. *Philos Trans R Soc Lond B Biol Sci*. 2013; 368. doi: 10.1098/rstb.2013.0010
- Motegi F, Sugimoto A. Sequential functioning of the ECT-2 RhoGEF, RHO-1 and CDC-42 establishes cell polarity in *Caenorhabditis elegans* embryos. *Nat Cell Biol*. 2006; 8:978–985. DOI: 10.1038/ncb1459
- Motegi F, Zonies S, Hao Y, Cuenca AA, Griffin E, Seydoux G. Microtubules induce self-organization of polarized PAR domains in *Caenorhabditis elegans* zygotes. *Nat Cell Biol*. 2011; 13:1361–1367. DOI: 10.1038/ncb2354 [PubMed: 21983565]
- Munro EM. PAR proteins and the cytoskeleton: a marriage of equals. *Curr Opin Cell Biol*. 2006; 18:86–94. DOI: 10.1016/j.ceb.2005.12.007 [PubMed: 16364625]
- Munro E, Bowerman B. Cellular symmetry breaking during *Caenorhabditis elegans* development. *Cold Spring Harb Perspect Biol*. 2009; 1. doi: 10.1101/cshperspect.a003400
- Munro E, Nance J, Priess JR. Cortical flows powered by asymmetrical contraction transport PAR proteins to establish and maintain anterior-posterior polarity in the early *C. elegans* embryo. *Dev Cell*. 2004; 7:413–424. DOI: 10.1016/j.devcel.2004.08.001 [PubMed: 15363415]

- Nelson WJ. Adaptation of core mechanisms to generate cell polarity. *Nature*. 2003; 422:766–774. DOI: 10.1038/nature01602 [PubMed: 12700771]
- Nishikawa M, Naganathan SR, Jülicher F, Grill SW. Controlling contractile instabilities in the actomyosin cortex. *eLife*. 2017; 6:e30537.doi: 10.7554/eLife.30537 [PubMed: 28722650]
- Noatynska A, Panbianco C, Gotta M. SPAT-1/Bora acts with Polo-like kinase 1 to regulate PAR polarity and cell cycle progression. *Development*. 2010; 137:3315–3325. DOI: 10.1242/dev.055293 [PubMed: 20823068]
- O'Connell KF, Maxwell KN, White JO. The *spd-2* gene is required for polarization of the anteroposterior axis and formation of the sperm asters in the *Caenorhabditis elegans* zygote. *Dev Biol*. 2000; 222:55–70. DOI: 10.1006/dbio.2000.9714 [PubMed: 10885746]
- özlü N, Srayko M, Kinoshita K, Habermann B, O'Toole ET, Müller-Reichert T, Schmalz N, Desai A, Hyman AA. An essential function of the *C. elegans* ortholog of TPX2 is to localize activated aurora A kinase to mitotic spindles. *Dev Cell*. 2005; 9:237–248. DOI: 10.1016/j.devcel.2005.07.002 [PubMed: 16054030]
- Pellettieri J, Seydoux G. Anterior-posterior polarity in *C. elegans* and *Drosophila* — PARAllels and differences. *Science*. 2002; 298:1946–1951. DOI: 10.1126/science.1072162 [PubMed: 12471246]
- Portier N, Audhya A, Maddox PS, Green RA, Dammermann A, Desai A, Oegema K. A microtubule-independent role for centrosomes and aurora a in nuclear envelope breakdown. *Dev Cell*. 2007; 12:515–529. DOI: 10.1016/j.devcel.2007.01.019 [PubMed: 17419991]
- Prokopenko SN, Brumby A, O'Keefe L, Prior L, He Y, Saint R, Bellen HJ. A putative exchange factor for Rho1 GTPase is required for initiation of cytokinesis in *Drosophila*. *Genes Dev*. 1999; 13:2301–2314. DOI: 10.1101/gad.13.17.2301 [PubMed: 10485851]
- Rappleye CA, Tagawa A, Lyczak R, Bowerman B, Aroian RV. The Anaphase-Promoting Complex and Separin are required for embryonic anterior-posterior axis formation. *Dev Cell*. 2002; 2:195–206. DOI: 10.1016/S1534-5807(02)00114-4 [PubMed: 11832245]
- Rappleye CA, Tagawa A, Le Bot N, Ahringer J, Aroian RV. Involvement of fatty acid pathways and cortical interaction of the pronuclear complex in *Caenorhabditis elegans* embryonic polarity. *BMC Dev Biol*. 2003; 3:8.doi: 10.1186/1471-213X-3-8 [PubMed: 14527340]
- Reboutier D, Troadec M-B, Cremet J-Y, Chauvin L, Guen V, Salaun P, Prigent C. Aurora A is involved in central spindle assembly through phosphorylation of Ser19 in P150Glued. *J Cell Biol*. 2013; 201:65–79. DOI: 10.1083/jcb.201210060
- Reese KJ, Dunn MA, Waddle JA, Seydoux G. Asymmetric segregation of PIE-1 in *C. elegans* is mediated by two complementary mechanisms that act through separate PIE-1 protein domains. *Mol Cell*. 2000; 6:445–455. DOI: 10.1016/S1097-2765(00)00043-5 [PubMed: 10983990]
- Reich JD, Hubatsch L, Illukkumbura R, Peglion F, Bland T, Hirani N, Goehring NW. Regulated activation of the PAR polarity network ensures a timely and specific response to spatial cues. *Curr Biol*. 2019; 29:1911–1923. DOI: 10.1016/j.cub.2019.04.058 [PubMed: 31155349]
- Rosa A, Vlassaks E, Pichaud F, Baum B. Ect2/Pbl acts via Rho and polarity proteins to direct the assembly of an isotropic actomyosin cortex upon mitotic entry. *Dev Cell*. 2015; 32:604–616. DOI: 10.1016/j.devcel.2015.01.012 [PubMed: 25703349]
- Rose L, Gönczy P. Polarity establishment, asymmetric division and segregation of fate determinants in early *C. elegans* embryos. *WormBook*. 2014; :1–43. DOI: 10.1895/wormbook.1.30.2
- Schonegg S, Hyman AA. CDC-42 and RHO-1 coordinate actomyosin contractility and PAR protein localization during polarity establishment in *C. elegans* embryos. *Development*. 2006; 133:3507–3516. DOI: 10.1242/dev.02527 [PubMed: 16899536]
- Schumacher JM, Ashcroft N, Donovan PJ, Golden A. A highly conserved centrosomal kinase, AIR-1, is required for accurate cell cycle progression and segregation of developmental factors in *Caenorhabditis elegans* embryos. *Development*. 1998; 125:4391–4402. [PubMed: 9778499]
- Seki A, Coppinger JA, Jang C-Y, Yates JR, Fang G. Bora and the kinase aurora A cooperatively activate the kinase Plk1 and control mitotic entry. *Science*. 2008; 320:1655–1658. DOI: 10.1126/science.1157425 [PubMed: 18566290]
- Severson AF, Bowerman B. Myosin and the PAR proteins polarize microfilament-dependent forces that shape and position mitotic spindles in *Caenorhabditis elegans*. *J Cell Biol*. 2003; 161:21–26. DOI: 10.1083/jcb.200210171 [PubMed: 12695495]

- Siegrist SE, Doe CQ. Microtubule-induced cortical cell polarity. *Genes Dev.* 2007; 21:483–496. DOI: 10.1101/gad.1511207 [PubMed: 17344411]
- Srayko M, Quintin S, Schwager A, Hyman AA. *Caenorhabditis elegans* TAC-1 and ZYG-9 form a complex that is essential for long astral and spindle microtubules. *Curr Biol.* 2003; 13:1506–1511. DOI: 10.1016/S0960-9822(03)00597-9 [PubMed: 12956952]
- St Johnston D. Establishing and transducing cell polarity: common themes and variations. *Curr Opin Cell Biol.* 2018; 51:33–41. DOI: 10.1016/j.ceb.2017.10.007 [PubMed: 29153703]
- Su K-C, Takaki T, Petronczki M. Targeting of the RhoGEF Ect2 to the equatorial membrane controls cleavage furrow formation during cytokinesis. *Dev Cell.* 2011; 21:1104–1115. DOI: 10.1016/j.devcel.2011.11.003 [PubMed: 22172673]
- Subramaniam K, Seydoux G. *nos-1* and *nos-2*, two genes related to *Drosophila nanos*, regulate primordial germ cell development and survival in *Caenorhabditis elegans*. *Development.* 1999; 126:4861–4871. [PubMed: 10518502]
- Tatsumoto T, Xie X, Blumenthal R, Okamoto I, Miki T. Human Ect2 is an exchange factor for Rho Gtpases, phosphorylated in G2/M phases, and involved in cytokinesis. *J Cell Biol.* 1999; 147:921–928. DOI: 10.1083/jcb.147.5.921 [PubMed: 10579713]
- Toji S, Yabuta N, Hosomi T, Nishihara S, Kobayashi T, Suzuki S, Tamai K, Nojima H. The centrosomal protein Lats2 is a phosphorylation target of Aurora-A kinase. *Genes Cells.* 2004; 9:383–397. DOI: 10.1111/j.1356-9597.2004.00732.x [PubMed: 15147269]
- Toya M, Terasawa M, Nagata K, Iida Y, Sugimoto A. A kinase-independent role for Aurora A in the assembly of mitotic spindle microtubules in *Caenorhabditis elegans* embryos. *Nat Cell Biol.* 2011; 13:708–714. DOI: 10.1038/ncb2242 [PubMed: 21572421]
- Tsai MC, Ahringer J. Microtubules are involved in anterior-posterior axis formation in *C. elegans* embryos. *J Cell Biol.* 2007; 179:397–402. DOI: 10.1083/jcb.200708101
- Tsai M-Y, Zheng Y. Aurora A kinase-coated beads function as microtubule-organizing centers and enhance RanGTP-induced spindle assembly. *Curr Biol.* 2005; 15:2156–2163. DOI: 10.1016/j.cub.2005.10.054 [PubMed: 16332542]
- Tse YC, Werner M, Longhini KM, Labbe J-C, Goldstein B, Glotzer M. RhoA activation during polarization and cytokinesis of the early *Caenorhabditis elegans* embryo is differentially dependent on NOP-1 and CYK-4. *Mol Biol Cell.* 2012; 23:4020–4031. DOI: 10.1091/mbc.e12-04-0268 [PubMed: 22918944]
- Wallenfang MR, Seydoux G. Polarization of the anterior-posterior axis of *C. elegans* is a microtubule-directed process. *Nature.* 2000; 408:89–92. DOI: 10.1038/35040562 [PubMed: 11081513]
- Walter AO, Seghezzi W, Korver W, Sheung J, Lees E. The mitotic serine/threonine kinase Aurora2/AIK is regulated by phosphorylation and degradation. *Oncogene.* 2000; 19:4906–4916. DOI: 10.1038/sj.onc.1203847 [PubMed: 11039908]
- Wong J, Lerrigo R, Jang C-Y, Fang G. Aurora A regulates the activity of HURP by controlling the accessibility of its microtubule-binding domain. *Mol Biol Cell.* 2008; 19:2083–2091. DOI: 10.1091/mbc.e07-10-1088 [PubMed: 18321990]
- Woodruff JB, Ferreira Gomes B, Widlund PO, Mahamid J, Honigsmann A, Hyman AA. The centrosome is a selective condensate that nucleates microtubules by concentrating tubulin. *Cell.* 2017; 169:1066–1077. DOI: 10.1016/j.cell.2017.05.028 [PubMed: 28575670]
- Yüce O, Piekny A, Glotzer M. An ECT2-centralspindlin complex regulates the localization and function of RhoA. *J Cell Biol.* 2005; 170:571–582. DOI: 10.1083/jcb.200501097
- Zeng K, Bastos RN, Barr FA, Gruneberg U. Protein phosphatase 6 regulates mitotic spindle formation by controlling the T-loop phosphorylation state of Aurora A bound to its activator TPX2. *J Cell Biol.* 2010; 191:1315–1332. DOI: 10.1083/jcb.201008106 [PubMed: 21187329]
- Zhang X, Ems-McClung SC, Walczak CE. Aurora A phosphorylates MCAK to control ran-dependent spindle bipolarity. *Mol Biol Cell.* 2008; 19:2752–2765. DOI: 10.1091/mbc.e08-02-0198 [PubMed: 18434591]
- Zhao P, Teng X, Tantirimudalige SN, Nishikawa M, Wohland T, Toyama Y, Motegi F. Aurora-A breaks symmetry in contractile actomyosin networks independently of its role in centrosome maturation. *Dev Cell.* 2019; 48:631–645. DOI: 10.1016/j.devcel.2019.02.012 [PubMed: 30861375]

Zonies S, Motegi F, Hao Y, Seydoux G. Symmetry breaking and polarization of the *C. elegans* zygote by the polarity protein PAR-2. *Development*. 2010; 137:1669–1677. DOI: 10.1242/dev [PubMed: 20392744]

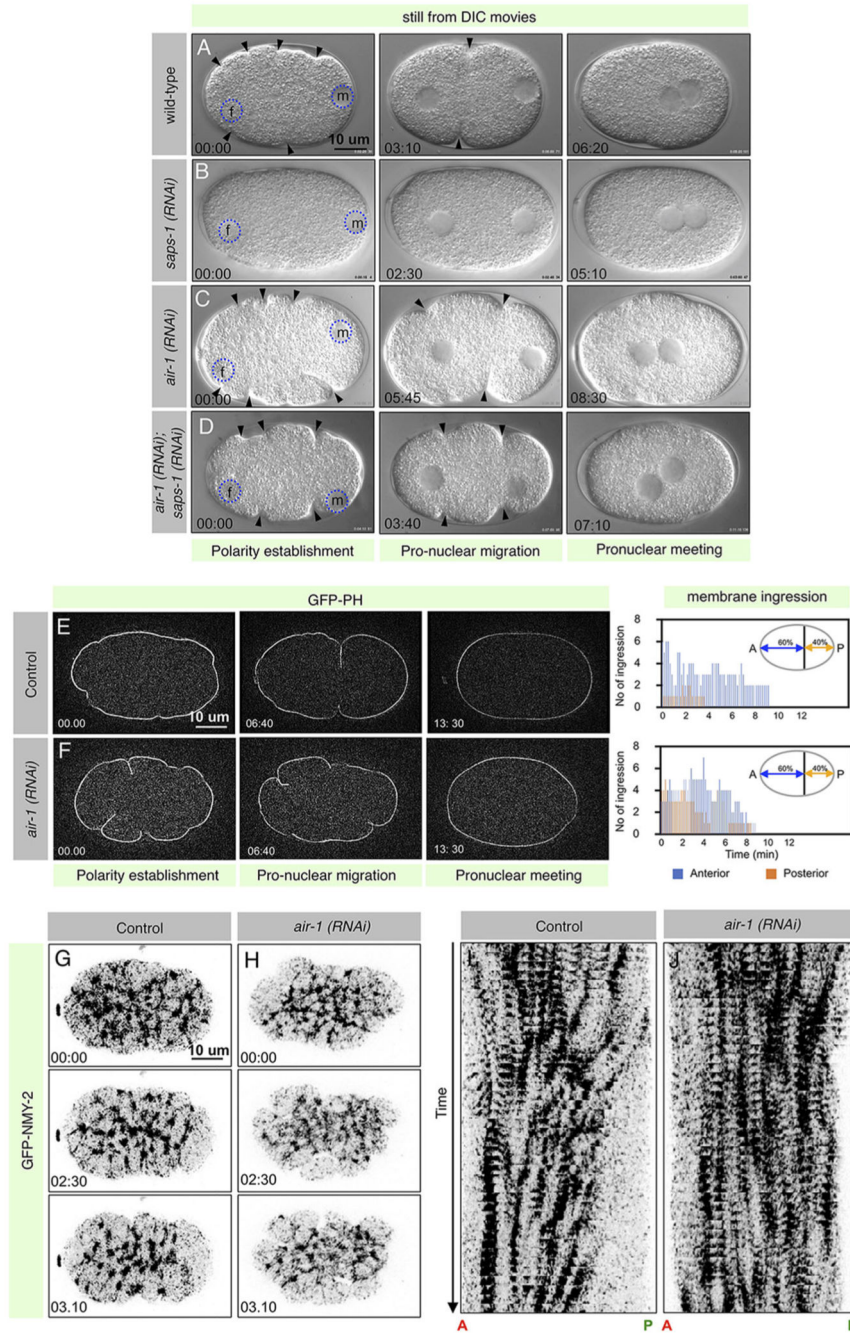


Fig. 1. Aurora A kinase (AIR-1) depletion causes excess cortical contractility in early one-cell stage embryos.

(A-D) Images from time-lapse differential interference contrast (DIC) microscopy of *C. elegans* early embryos in wild-type (A), *saps-1(RNAi)* (B), *air-1(RNAi)* (C) or *air-1 (RNAi); saps-1 (RNAi)* (D). See also corresponding Movies 1,2,5 and 6. In this and subsequent images, embryos are ~50 μ m in length and the posterior is to the right. Blue dashed circles highlight the male (m) and female (f) pronuclei; the black arrowheads represent cortical ruffles. In this and other DIC images, if not specified, time is shown in minutes standardised by the size of the male pronucleus and appearance of the posterior smoothing with t=0

corresponding to the size equivalent of 5-6 μm (see Materials and Methods for details). There is excess cortical contractility in the *air-1 (RNAi)* embryo either alone or together with *saps-1 (RNAi)*, in contrast to the wild-type embryo. In addition, cortical contractility is significantly diminished in the *saps-1 (RNAi)* embryo. More than 50 embryos were analysed for each condition; the images from the representative embryos are shown. (E,F) Images from time-lapse confocal microscopy of embryos expressing GFP-PH in control (E) and in *air-1 (RNAi)* (F) at the various stages. See also corresponding Movies 7 and 8. Time is represented in minutes, with t=0 corresponding to the frame from where the imaging was initiated, i.e. approximately the time of polarity establishment just a few minutes after meiosis II completion. There are excess membrane ruffles in the *air-1(RNAi)* embryo in comparison with the control embryo. Quantification on the right represents membrane ingression in 60% of the anterior (A) region (shown in blue) and the 40% of the posterior (P) region (shown in orange) of the embryo. In the control embryo, the posterior ingression diminishes very early and is absent at the time of pronuclear migration. However, such ingressions stay for much longer and disappear together with the anterior ingression in *air-1 (RNAi)*. Ten embryos were analysed for each condition; representative embryos are shown. (G-J) Cortical images (G,H) and the Kymograph analysis (I,J; see Materials and Methods) from time-lapse confocal microscopy of embryos expressing GFP-NMY-2 in control (G,I) and in *air-1 (RNAi)* (H,J). See also corresponding Movies 9 and 10. Time is represented in minutes, with t=0 corresponding to the frame from where the imaging was initiated, i.e. approximately the time of polarity establishment just a few minutes after meiosis II completion. In the control embryo, the GFP-NMY-2 foci move from the posterior (P) to the anterior (A) surface, which is not the case in *air-1 (RNAi)* at early time points. In addition, there is GFP-NMY-2 clearance at the extreme anterior and posterior parts of the embryo in *air-1 (RNAi)* (see Movie 10). More than ten embryos were recorded; representative embryos are shown.

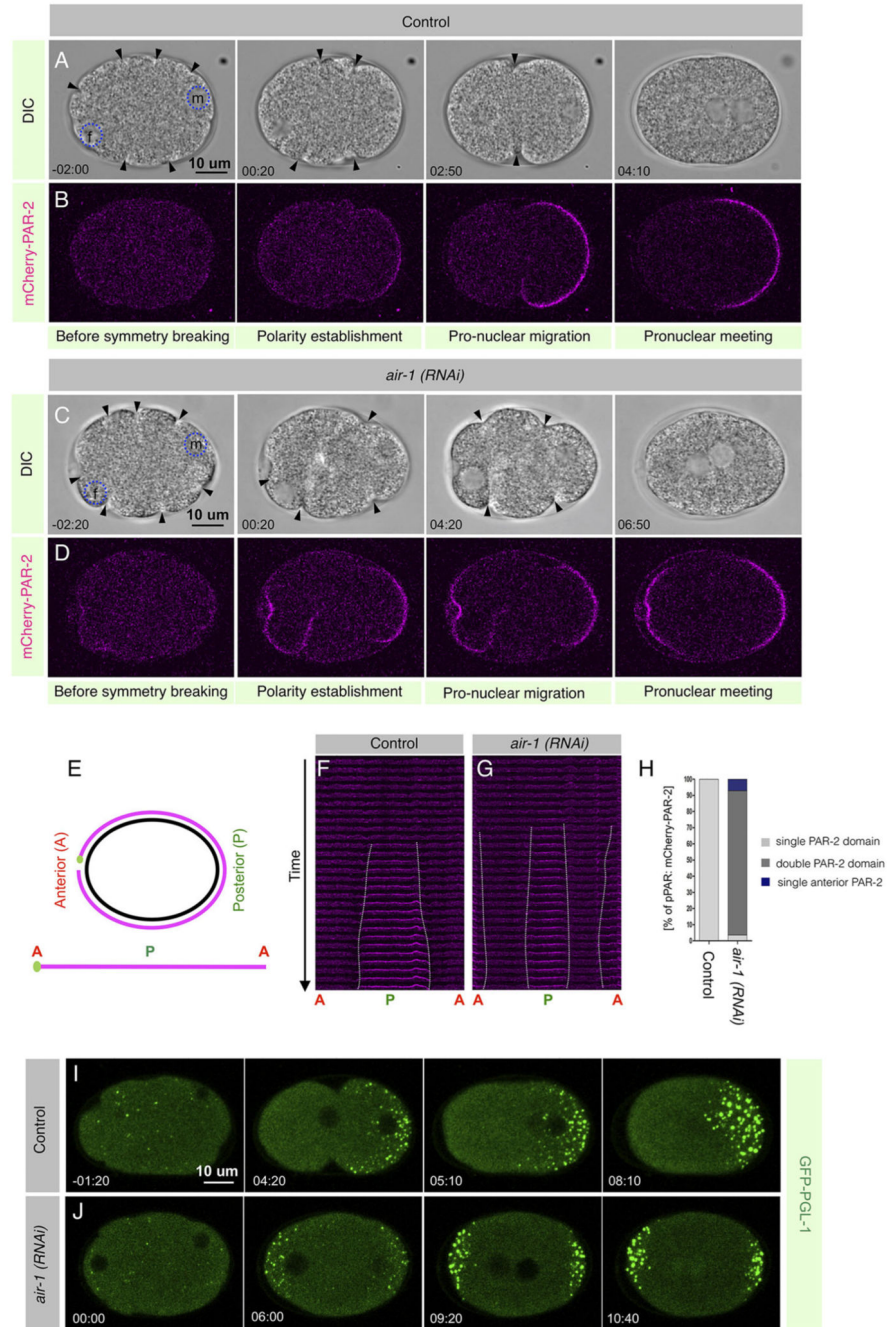


Fig. 2. AIR-1 blocks multiple polarisation events in the one-cell embryo.

(A-D) Images from time-lapse confocal microscopy in combination with DIC microscopy of embryos expressing mCherry-PAR-2 in control (A,B) or in *air-1 (RNAi)* (C,D) at the various stages. See also corresponding Movies 11 and 12. mCherry-PAR-2 signal is shown in magenta. There are excess membrane ruffles (arrowheads) in the *air-1(RNAi)* embryo in comparison with the control embryo. The appearance of two PAR-2 domains at the anterior and posterior cell cortex in the *air-1 (RNAi)* embryo differs from the single posterior PAR-2 domain in the control embryo. In this and other images from one-cell embryos expressing

either mCherry-PAR-2 or GFP-PAR-2, if not specified, time is shown in minutes standardised by the size of the male pronucleus and the onset of PAR-2 enrichment at the posterior cortex with $t=0$ corresponding to the male pronucleus being ~5-6 μm in diameter. Blue dashed circles highlight the male (m) and female (f) pronuclei. Fifty embryos were recorded; the representative embryos are shown. (E) Schematic of an embryo where the cortical surface (magenta) is straightened from anterior to posterior to anterior to analyse the mCherry-PAR-2 localisation in the form of kymographs as shown in F and G. (F,G) Cortical localisation of mCherry-PAR-2 signal from the time-lapse confocal images from the 8-10 frames before polarisation until the initiation of the pseudocleavage in the one-cell of control embryo or *air-1 (RNAi)* for the analogous timings. mCherry-PAR-2 signal appears at the A and P cortical regions in *air-1 (RNAi)*, in contrast to control embryos. The timing of PAR-2 domain appearance in *air-1 (RNAi)* embryos is similar to that in control embryos. See Materials and Methods for details. (H) Quantification of the positioning of the PAR-2 domain appearance in control and in embryos depleted of AIR-1. Two PAR-2 axes are formed in ~90% of the *air-1 (RNAi)* embryos, in contrast to none in control embryos. Around 7% of AIR-1-depleted embryos also show the appearance of the single anterior PAR-2 domain. $n=50$. (I,J) Images from time-lapse epifluorescence microscopy of embryos expressing the P-granule component GFP-PGL-1 in control (I) or in *air-1 (RNAi)* (J). GFP-PGL-1 signal is shown in green. See also corresponding Movies 19 and 20. Two GFP-PGL-1-enriched regions are present in *air-1 (RNAi)* embryos compared with control embryos. More than ten embryos were recorded; the representative embryos are shown.

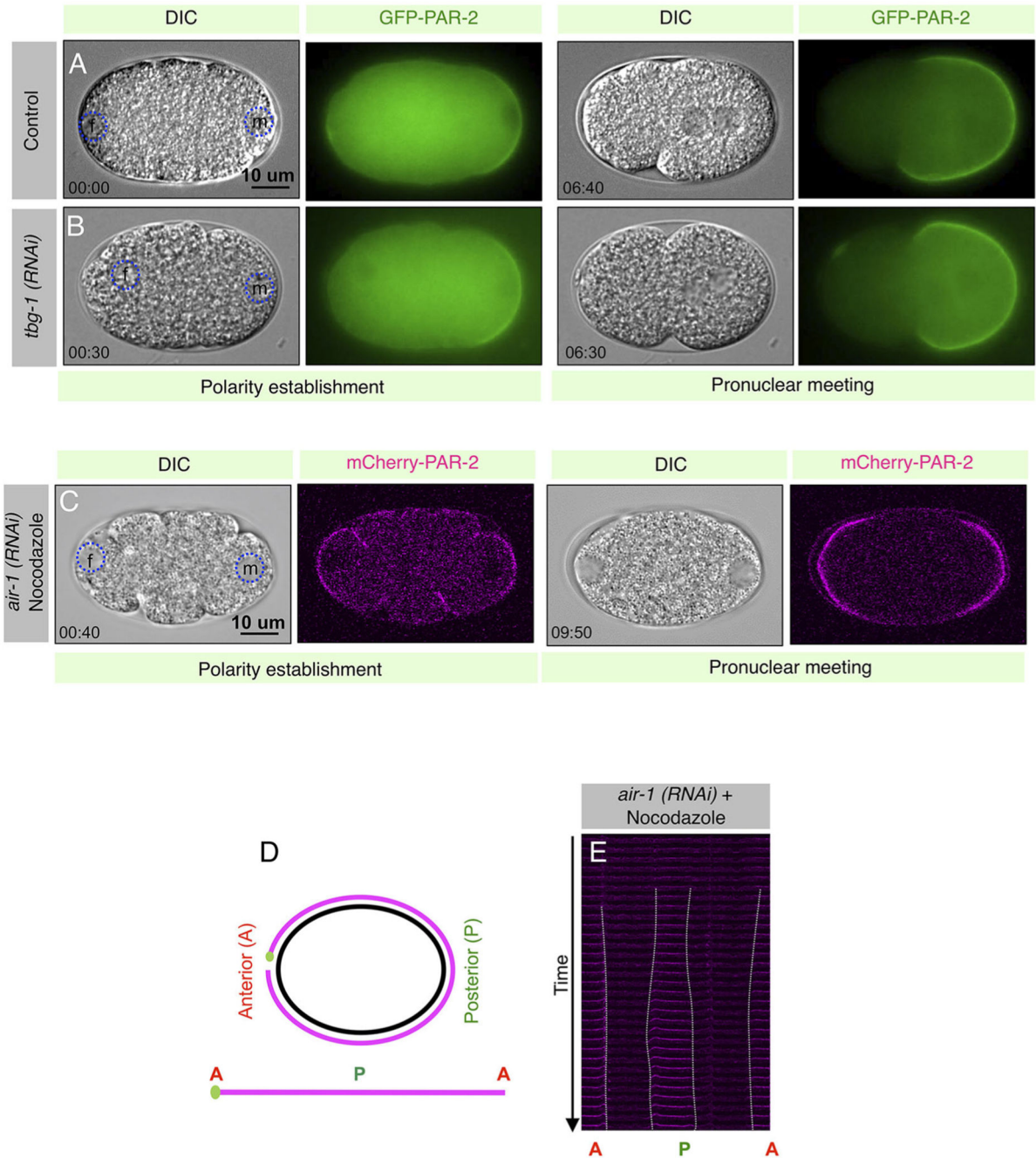


Fig. 3. AIR-1 microtubule nucleation function is not crucial for blocking promiscuous PAR-2.

(A,B) Images from time-lapse epifluorescence microscopy in combination with DIC microscopy of embryos expressing GFP-PAR-2 in control (A) or in *tbg-1 (RNAi)* (B). GFP-PAR-2 signal is shown in green. More than ten embryos were recorded, and the representative embryos are shown [see also the *tbg-1 (RNAi)* phenotype in Fig. S1C, with quantification in Fig.S1E and Movie 23]. (C) Images from time-lapse confocal microscopy in combination with DIC microscopy of embryos expressing mCherry-PAR-2 in *air-1 (RNAi)* embryos that are also treated with the microtubule poison nocodazole (see also

corresponding Movie 25). mCherry-PAR-2 signal is shown in magenta. The pronuclei do not migrate and stay close to the anterior and posterior cortex at the pronuclear meeting stage because of the diminished microtubule asters in *air-1 (RNAi)* embryos that are treated with nocodazole (see also the impact of on microtubules in Fig. S1D; quantification in Fig. S1E; Movie 24). Blue dashed circles highlight the male (m) and female (f) pronuclei. More than ten embryos were recorded, and the representative embryos are shown. (D) Schematic of an embryo, as demonstrated for Fig. 2C, for analysing mCherry-PAR-2 localisation over time in the form of a kymograph. (E) Cortical localisation of mCherry-PAR-2 signal from the time-lapse confocal images from five frames before polarisation until the initiation of the pseudocleavage in *air-1 (RNAi)* one-cell embryos that are also treated with nocodazole. mCherry-PAR-2 signal appears at the anterior (A) as well as posterior (P) cortical region in 100% of *air-1 (RNAi)* plus nocodazole embryos. $n=10$. See also Movie 25.

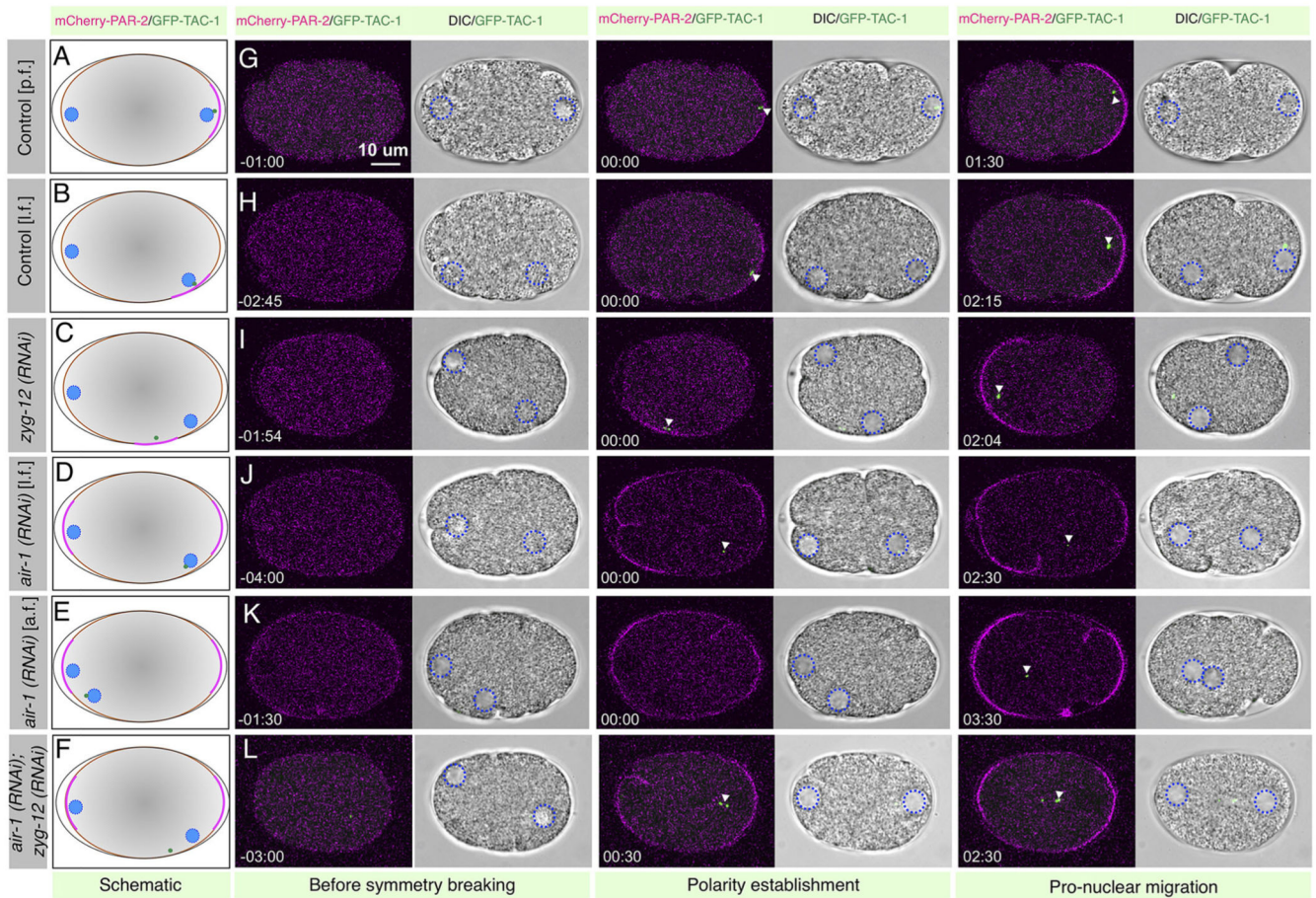


Fig. 4. Centrosomes are dispensable for guiding pPAR axis formation in embryos depleted of AIR-1.

(A-L) Schematics of the embryos on the left (A-F) represent the various conditions and their corresponding images on the right (G-L) from time-lapse confocal microscopy in combination with DIC microscopy of embryos co-expressing mCherry-PAR-2 and GFP-TAC-1. Control embryo that underwent posterior fertilisation [p.f.] (A,G), control embryo that underwent lateral fertilisation [l.f.] (B,H), embryo depleted of ZYG-12 (a member of the Hook family of cytoskeletal linker proteins; C,I), *air-1 (RNAi)* embryo that underwent lateral fertilisation (D,J), *air-1 (RNAi)* embryo that underwent anterior fertilisation (E,K) and *air-1 (RNAi); zyg-12 (RNAi)* embryo (F,L) in the early one-cell stages. See also corresponding Movies 27-32. In schematic representations, filled blue circles represent female and male pronuclei, magenta on the cell cortex represents PAR-2 localisation and the small green circle marks the centrosomes. In confocal images, the white arrowhead represents the position of the centrosomes. mCherry-PAR-2 signal is shown in magenta and GFP-TAC-1 is in green. In *zyg-12 (RNAi)*, the centrosomes are not anchored on the nuclear membrane and the position of such an unanchored centrosome is sufficient to drive mCherry-PAR-2 localisation to the anterior. *air-1(RNAi)* embryos that underwent lateral fertilisation or anterior fertilisation, or in which centrosomes are unable to anchor at the nuclear envelope [e.g. in *zyg-12 (RNAi)*], show anterior and posterior PAR-2 domains irrespective of the position of the centrosomes. More than ten embryos were recorded for

each condition, except where the embryos underwent anterior fertilisation, where $n=5$; representative embryos are shown.

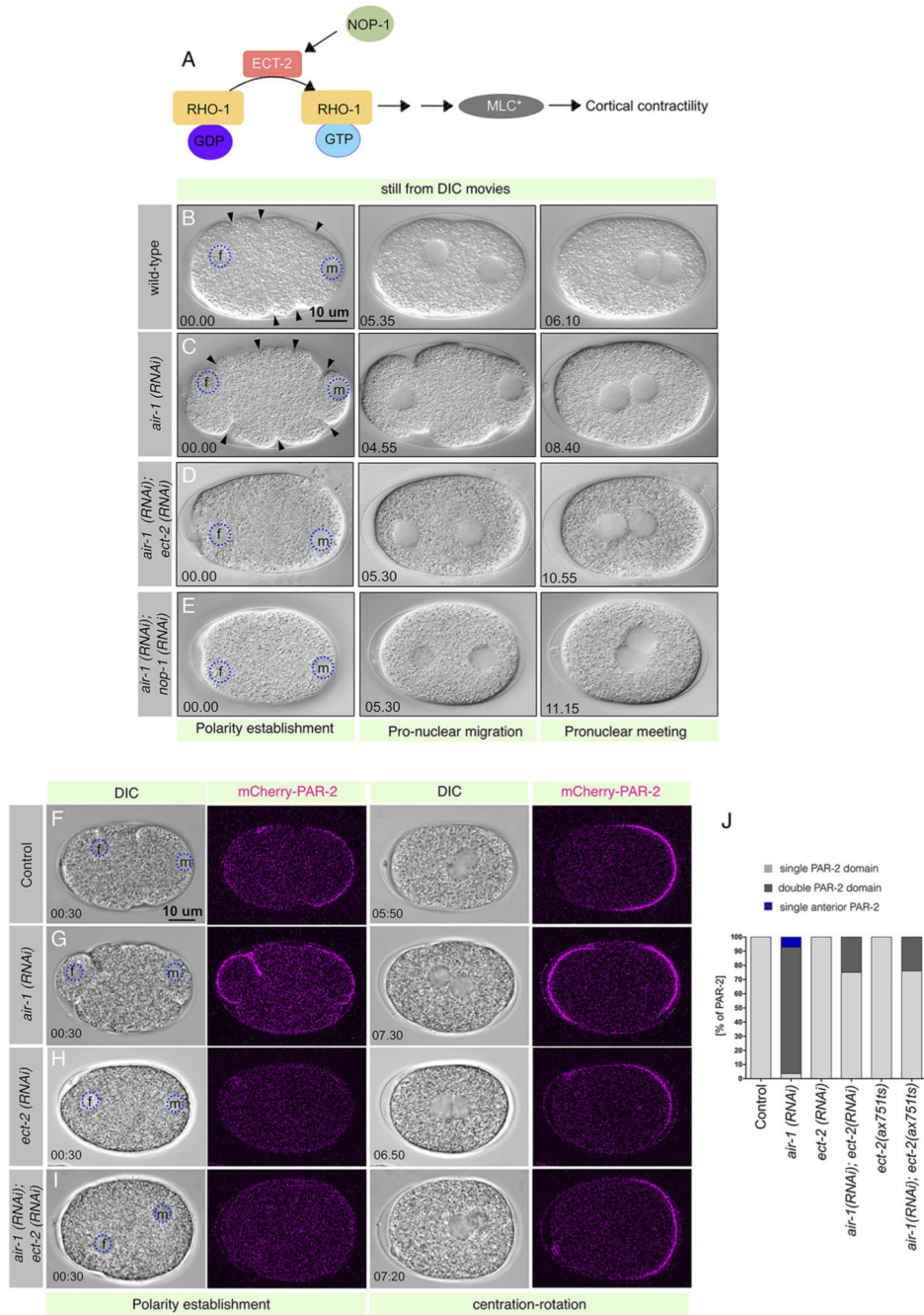


Fig. 5. ECT-2 and its activator NOP-1 act downstream of AIR-1.

(A) Schematic representation of the pathway regulating cortical contractility through myosin activity [represented by phosphorylated myosin light chain (MLC*)] in the one-cell embryo. (B-E) Images from time-lapse DIC microscopy of early embryos in wild type (B), *air-1(RNAi)* (C), *air-1 (RNAi); ect-2 (RNAi)* (D) and *air-1 (RNAi); nop-1 (RNAi)* (E). There is excess cortical contractility in the *air-1(RNAi)* embryo (arrowheads) that is diminished in *air-1 (RNAi); ect-2 (RNAi)* or *air-1 (RNAi); nop-1 (RNAi)* embryos. Time is shown in minutes which is solely based on the size of the male pronucleus because of the absence of

cortical contractility in *ect-2 (RNAi)* or *nop-1 (RNAi)* alone or in combination with *air-1 (RNAi)*. $t=0$ corresponding to the size equivalent of 5-6 μm of the male pronucleus. Ten embryos were analysed for each condition; representative embryos are shown. Blue dashed circles highlight the male (m) and female (f) pronuclei. (F-I) Images from time-lapse confocal microscopy in combination with DIC microscopy of embryos expressing mCherry-PAR-2 in control (F), *air-1 (RNAi)* (G), *ect-2 (RNAi)* (H) and *air-1 (RNAi); ect-2 (RNAi)* (I) at the various stages indicated. See also corresponding Movies 33-36. mCherry-PAR-2 signal is shown in magenta. An extra PAR-2 domain is present at the anterior in *air-1 (RNAi)* but lost in *air-1(RNAi); ect-2 (RNAi)* embryos (see quantification in J). In *ect-2 (RNAi)* or in *air-1(RNAi) ect-2 (RNAi)*, the appearance of the posterior PAR-2 domain is significantly delayed in 100% of the embryo in contrast to control embryos [as reported previously for ECT-2 depletion (see Fig. S5E and Tse et al., 2012)]. The efficiency of the double depletion of in *ect-2 (RNAi); air-1 (RNAi)*, as monitored by various means, is shown in Figs S6 and S7. (J) Quantification of the positioning of the PAR-2 domain in control, *air-1(RNAi)*, *ect-2 (RNAi)* and *air-1 (RNAi); ect-2 (RNAi)*, and in a temperature-sensitive *ect-2 (ax751 ts)* mutant that is either non-treated or treated with *air-1 (RNAi)* at the restrictive temperature at the time of centration rotation. Fig. S7E-H contains the *ect-2 (ax751 ts)* mutant data. More than 15 embryos were recorded for each condition.

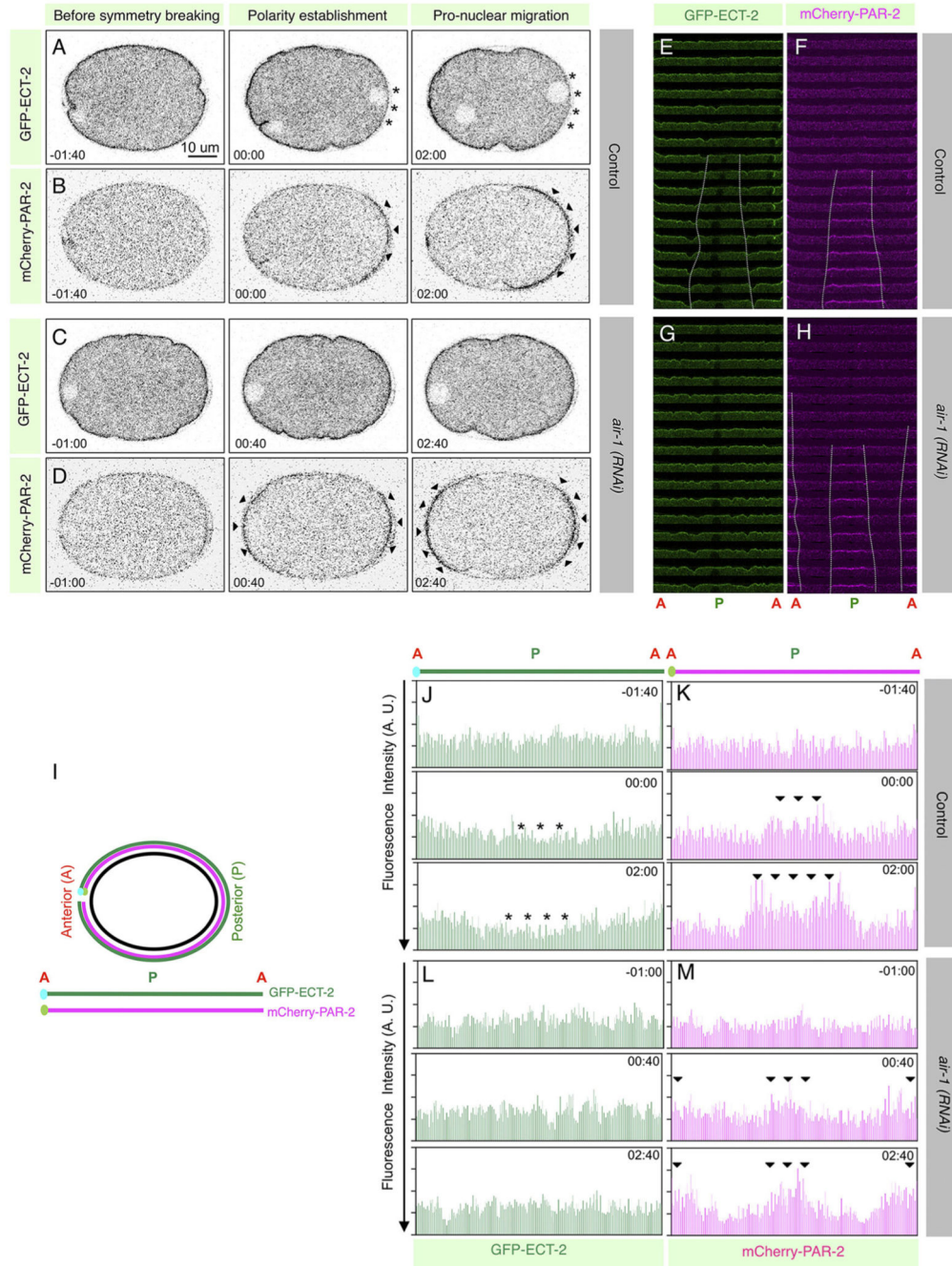


Fig. 6. AIR-1 delocalises ECT-2 at the posterior cortex at the time corresponding to polarity establishment.

(A-D) Inverted contrast images from time-lapse confocal microscopy of one-cell embryos co-expressing mCherry-PAR-2 and GFP-ECT-2 in control (A,B) or *air-1* (RNAi) (C,D) at various stages. mCherry-PAR-2 and GFP-ECT-2 signal is shown in grey. See also corresponding Movies 37 and 38. GFP-ECT-2 delocalises at the posterior cortex at the time of symmetry breaking in the one-cell embryo and a concomitant mCherry-PAR-2 signal appears at the posterior cortex. In the *air-1* (RNAi), two PAR-2 axes are established and ECT-2 does not delocalise from the posterior cortex. More than ten embryos were recorded;

the representative embryos are shown. Asterisks represent GFP-ECT-2 exclusion; black arrowheads represent the appearance of mCherry-PAR-2 signal. (E-H) Cortical localisation of GFP-ECT-2 and mCherry-PAR-2 signal from the time-lapse confocal images starting from the eight frames before polarisation until the initiation of the pseudocleavage in the one-cell embryo (as shown for Fig. 2E-G). GFP-ECT-2 exclusion coincides with the appearance of mCherry-PAR-2 at the posterior cell cortex in the control embryo. GFP-ECT-2 signal is not diminished from the posterior cortex in *air-1 (RNAi)* and mCherry-PAR-2 signal appears at the anterior (A) as well as posterior (P) cortical surfaces. (I) Schematic of an embryo where the cortical surface (green for GFP-ECT-2 or magenta for mCherry-PAR-2) is straightened from anterior to posterior to anterior to analyse the cortical fluorescence intensity over time. (J-M) Line scan analysis of the fluorescence intensities in arbitrary units (A.U.) for the cortical GFP-ECT-2 (in green) or mCherry-PAR-2 (in magenta) for the images shown in A-D in control (J,K) or *air-1 (RNAi)* (L,M). Asterisks represent the cortical region that is depleted of GFP-ECT-2; black arrowheads represent the cortical region where mCherry-PAR-2 signal appears in the embryos. The appearance of mCherry-PAR-2 coincides with the loss of cortical GFP-ECT-2 in control embryos.

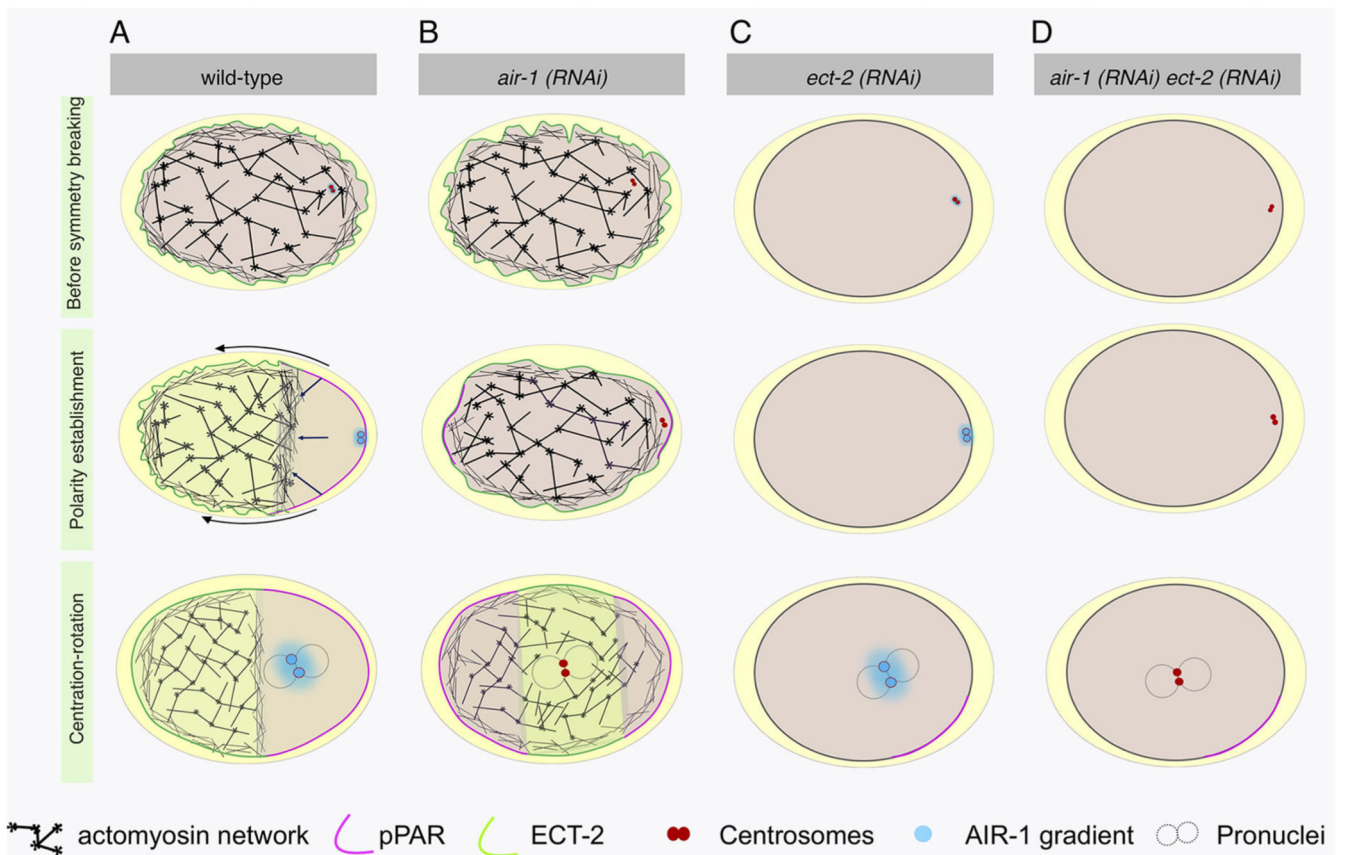


Fig. 7. AIR-1 is essential in ensuring a single pPAR-2 axis.

(A-D) Working model for the function of AIR-1 in regulating a single polarity axis at the time of polarity establishment in the one-cell embryo. In the wild type, before the symmetry-breaking event, the entire embryo surface is undergoing contraction-relaxation and the RhoGEF, ECT-2 (in green) is localised at the cell membrane; PAR-2 (in magenta) is restricted to the cytoplasm. At the onset of polarity establishment, relaxation of the posterior cortex, presumably by the exclusion of ECT-2 from the surface close to the AIR-1 centrosomal gradient (in cyan), causes PAR-2 to localise at the posterior domain, thus enabling polarity establishment. At the centration-rotation stage, a well-defined PAR-2 domain is formed and ECT-2 is mainly restricted to the anterior embryo surface. (A) In *air-1 (RNAi)* embryos, excess cortical contractility is present because of the presence of ECT-2 at the entire surface; such contractility is not abolished at the time of polarity establishment and this causes the occurrence of a promiscuous PAR-2 domain at the anterior and posterior cortex (B). In contrast, in *ect-2 (RNAi)* or in *air-1 (RNAi) ect-2 (RNAi)* embryos, contractility is absent; these embryos are characterised by the appearance of the PAR-2 domain that is significantly delayed compared with the wild-type embryos (C,D). Centrosomes are shown in red.